Open Research Online

The Open University's repository of research publications
and other research outputs

Descent toward the icehouse: Eocene sea surface cooling inferred from GDGT distributions

Journal Item

For guidance on citations see FAQs.

oro.open.ac.uk

RESEARCH ARTICLE

Key Points:
- Archaea other than marine Thaumarchaeota exert a minimal impact on most Eocene temperatures
- Tropical and high-latitude cooling during the descent towards the icehouse
- Carbon dioxide is the most likely driver of long-term Eocene cooling

Descent toward the Icehouse: Eocene sea surface cooling inferred from GDGT distributions

Gordon N. Inglis[1,2], Alexander Farnsworth[2,3], Daniel Lunt[2,3], Gavin L. Foster[4], Christopher J. Hollis[5], Mark Pagani[6], Phillip E. Jardine[7], Paul N. Pearson[8], Paul Markwick[9], Amanda M. J. Galsworthy[9], Lauren Raynham[9], Kyle. W. R. Taylor[1,2], and Richard D. Pancost[1,2]

[1]Organic Geochemistry Unit, School of Chemistry, University of Bristol, Bristol, UK, [2]Cabot Institute, University of Bristol, Bristol, UK, [3]BRIDGE, School of Geographical Sciences, University of Bristol, Bristol, UK, [4]Ocean and Earth Science, National Oceanography Centre Southampton, University of Southampton Waterfront Campus, Southampton, UK, [5]Department of Paleontology, GNS Science, Wellington, New Zealand, [6]Department of Geology and Geophysics, Yale University, New Haven, Connecticut, USA, [7]Department of Environment, Earth & Ecosystems, Open University, Milton Keynes, UK, [8]School of Earth and Ocean Sciences, Cardiff University, Cardiff, UK, [9]Getech UK, Leeds, UK

Abstract The TEX_{86} proxy, based on the distribution of marine isoprenoidal glycerol dialkyl glycerol tetraether lipids (GDGTs), is increasingly used to reconstruct sea surface temperature (SST) during the Eocene epoch (56.0–33.9 Ma). Here we compile published TEX_{86} records, critically reevaluate them in light of new understandings in TEX_{86} palaeothermometry, and supplement them with new data in order to evaluate long-term temperature trends in the Eocene. We investigate the effect of archaea other than marine Thaumarchaeota upon TEX_{86} values using the branched-to-isoprenoid tetraether index (BIT), the abundance of GDGT-0 relative to crenarchaeol (%GDGT-0), and the Methane Index (MI). We also introduce a new ratio, %$GDGT_{RS}$, which may help identify Red Sea-type GDGT distributions in the geological record. Using the offset between TEX_{86}^{H} and TEX_{86}^{L} (ΔH-L) and the ratio between GDGT-2 and GDGT-3 ([2]/[3]), we evaluate different TEX_{86} calibrations and present the first integrated SST compilation for the Eocene (55 to 34 Ma). Although the available data are still sparse some geographic trends can now be resolved. In the high latitudes (>55°), there was substantial cooling during the Eocene (~6°C). Our compiled record also indicates tropical cooling of ~2.5°C during the same interval. Using an ensemble of climate model simulations that span the Eocene, our results indicate that only a small percentage (~10%) of the reconstructed temperature change can be ascribed to ocean gateway reorganization or paleogeographic change. Collectively, this indicates that atmospheric carbon dioxide (pCO$_2$) was the likely driver of surface water cooling during the descent toward the icehouse.

1. Introduction

Throughout the Phanerozoic, and possibly throughout geological time, the Earth's climate has oscillated between greenhouse and icehouse climate states, where greenhouse climates are characterized by high atmospheric carbon dioxide (pCO$_2$) [*Pearson and Palmer*, 2000; *Pagani et al.*, 2005; *Lowenstein and Demicco*, 2006; *Pearson et al.*, 2009], high sea surface temperatures (SST) [*Pearson et al.*, 2007; *Bijl et al.*, 2009; *Hollis et al.*, 2012], and the absence of continental ice sheets [*Francis and Poole*, 2002; *Contreras et al.*, 2013], and icehouse climates are characterized by the opposite: reduced pCO$_2$, reduced SST, and presence of continental ice sheets [*Zachos et al.*, 1992; *Pearson and Palmer*, 2000; *DeConto and Pollard*, 2003; *Pagani et al.*, 2005; *Lear et al.*, 2008; *Zhang et al.*, 2013]. The most recent transition, from a greenhouse to an icehouse climate state, occurred during the Eocene-Oligocene transition (EOT; ~33.6–34.1 Ma). It is thought to have been driven by either a long-term decline in pCO$_2$ [*Pagani et al.*, 2005; *Zhang et al.*, 2013] and/or changes in ocean circulation and heat distribution as a result of ocean gateway reorganization [*Kennett and Exon*, 2004; *Stickley et al.*, 2004; *Bijl et al.*, 2013]. The generation of long-term, regional temperature records is essential for developing a more detailed picture of global cooling during the Eocene and elucidating the driving mechanisms responsible.

TEX_{86}, an organic palaeothermometer based upon the distribution of isoprenoidal glycerol dialkyl glycerol tetraethers (GDGTs) in marine Thaumarchaeota, has previously been used to reconstruct spatial and temporal patterns of oceanic cooling during the Eocene [*Pearson et al.*, 2007; *Burgess et al.*, 2008; *Bijl et al.*, 2009; *Hollis et al.*, 2009; *Liu et al.*, 2009; *Hollis et al.*, 2012; *Bijl et al.*, 2013]. A recent TEX_{86} core-top

calibration introduced two separate indices and calibrations for (1) the entire data set (GDGT ratio-1; TEX_{86}^{L}) and (2) a subset of the data set that excluded GDGT distributions from high-latitude sediments (GDGT ratio-2; TEX_{86}^{H}) [*Kim et al.*, 2010]. *Kim et al.* [2010] recommended applying TEX_{86}^{H} when SSTs are estimated to have been above 15°C and TEX_{86}^{L} where SSTs may have ranged below 15°C. However, this approach has been questioned [*Taylor et al.*, 2013], and it is unclear which of the two calibrations is most appropriate for a given setting. The most recent TEX_{86} calibration is based upon the original TEX_{86} [*Schouten et al.*, 2002] and calibrated to SST using a spatially varying, Bayesian regression model (BAYSPAR) [*Tierney and Tingley*, 2014].

The TEX_{86} proxy is based upon the assumption that GDGTs in sediments are largely derived from Thaumarchaeota living in the upper water column [*Schouten et al.*, 2002; *Pearson and Ingalls*, 2013]. However, Thaumarchaeota are not restricted to these settings and inputs of GDGTs to sediments from alternative sources will affect TEX_{86} SST estimates. For example, Groups I.1a and I.1b Thaumarchaeota are present in the terrestrial environment [*Jurgens et al.*, 1997; *Ochsenreiter et al.*, 2003] and can bias TEX_{86} SST estimates in areas with high terrigenous input [*Hopmans et al.*, 2004; *Sluijs et al.*, 2006; *Weijers et al.*, 2006b; *Sluijs et al.*, 2009]. Considerable work has also explored the potential for sedimentary GDGT production to affect TEX_{86} values. Particular interest has focused upon methanotrophic [*Schouten et al.*, 2003; *Weijers et al.*, 2011; *Y. G. Zhang et al.*, 2011] and methanogenic [*Schouten et al.*, 2002; *Blaga et al.*, 2009] archaea, yet these sources are rarely discussed in deep-time investigations.

As Thaumarchaeota live throughout the water column [*Karner et al.*, 2001], it is also likely that subsurface archaea are exported to sediments [*Pearson et al.*, 2001; *Shah et al.*, 2008; *Taylor et al.*, 2013; *Hernández-Sánchez et al.*, 2014]. During the Eocene, unexpectedly large offsets between TEX_{86}^{H} and TEX_{86}^{L} (ΔH-L) are observed above 15°C [*Hollis et al.*, 2012]. The reason for this is unclear, but it has been argued that it could, in part, reflect enhanced export of archaea living in the subsurface with elevated ratios of GDGT-2 to GDGT-3 ([2]/[3] ratios) [*Taylor et al.*, 2013; *Kim et al.*, 2015].

Paleotemperature reconstructions based on TEX_{86} assume that Thaumarchaeota in modern oceans are representative of those living in ancient settings. In most open ocean settings, thaumarchaeotal assemblages are dominated by Group I.1a Thaumarchaeota [*Pester et al.*, 2011] which are the putative biological source of the sedimentary GDGTs that define the TEX_{86} core-top calibration. In the Red Sea, however, phylogenetically distinct archaeal communities occur both above and below the thermocline [*Eder et al.*, 2002; *Ionescu et al.*, 2009; *Qian et al.*, 2011] and correspond to core-top sediments in which TEX_{86} values consistently overestimate satellite-derived SST by 6–8°C [*Trommer et al.*, 2009].

Here, we critically evaluate new and previously published GDGT distributions from Eocene sediments in order to understand the drivers of long-term cooling. Using the Methane Index (MI) [*Y. G. Zhang et al.*, 2011], % GDGT-0 [*Sinninghe Damsté et al.*, 2012], and the branched and isoprenoidal tetraether (BIT) index [*Hopmans et al.*, 2004; *Weijers et al.*, 2006b], we assess the impact of archaea other than marine Thaumarchaeota upon Eocene TEX_{86} values. We also propose a new index (%GDGT$_{RS}$) which we use to tentatively identify Red Sea-type GDGT distributions within the geological record. We use ΔH-L offsets and [2]/[3] ratios [*Taylor et al.*, 2013] to suggest the most appropriate TEX_{86} calibration for a given setting. Based on those observations, we use new and previously published TEX_{86} SST estimates to reconstruct spatial patterns of cooling during the Eocene (55–34 Ma) and earliest Oligocene (33–34 Ma). We compare our results with an ensemble of climate model simulations and investigate the most likely driving mechanism of long-term cooling during the descent toward the icehouse.

2. Methods

2.1. Data Compilation

TEX_{86} indices were compiled from Deep Sea Drilling Project (DSDP) Site 277 [*Liu et al.*, 2009], DSDP Site 511 [*Liu et al.*, 2009], Ocean Drilling Program (ODP) Site 628 [*Liu et al.*, 2009], ODP Site 803 [*Liu et al.*, 2009], ODP Site 925 [*Liu et al.*, 2009], ODP Site 929 [*Liu et al.*, 2009], ODP Site 998 [*Liu et al.*, 2009], ODP Site 1218 [*Liu et al.*, 2009], ODP Site 1172 [*Bijl et al.*, 2009], ODP Site 913 [*Liu et al.*, 2009], International Ocean Drilling Program (IODP) Site 1356 [*Bijl et al.*, 2013], Tanzania (Tanzania Drilling Project: TDP [Sites 2, 3, 7, 12, 13, and 18]) [*Pearson et al.*, 2007], New Zealand (Hampden Beach and Mid-Waipara River) [*Burgess et al.*, 2008; *Hollis*
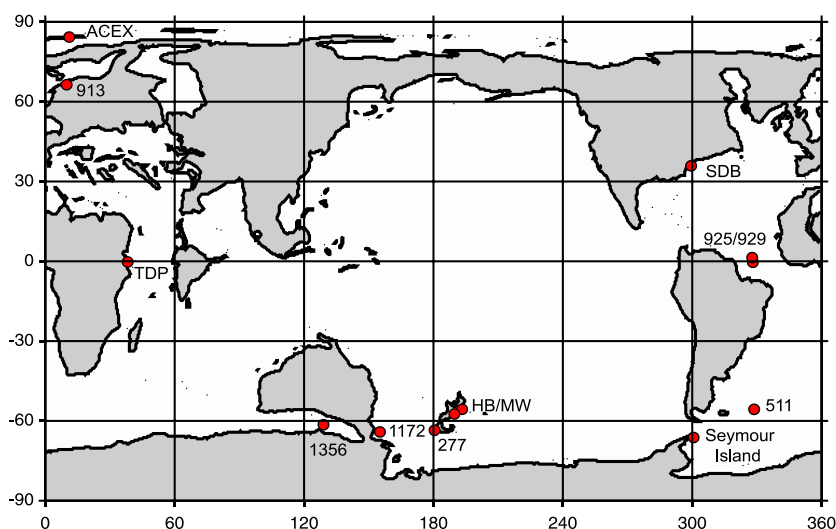
Figure 1. Palaeogeographic reconstruction of the early Eocene (56.0–47.8 Ma) with the location of each Eocene site used in this compilation.

et al., 2009; *Hollis et al.*, 2012], and the Arctic Coring Expedition (ACEX) [*Sluijs et al.*, 2006; *Sluijs et al.*, 2009] (Figure 1). Where possible, we calculate and report the fractional abundance of all individual GDGTs (see supporting information). All GDGT-based indices are reported relative to the Geologic Time Scale 2012 (GTS2012) [*Gradstein et al.*, 2012].

2.2. GDGT Analyses

To complement our data compilation, we have determined GDGT distributions from ODP Site 929 (Ceara Rise), ODP Site 913 (Greenland Basin), South Dover Bridge (Atlantic Coastal Plain), and Hampden Beach (New Zealand) using methods similar to those of previous studies [*Liu et al.*, 2009; *Hollis et al.*, 2012] (Figure 1). Approximately 35–70 g of ground sediment was extracted via Soxhlet apparatus for 24 h using dichloromethane/methanol (2:1 vol/vol) as the organic solvent. The total lipid extract was subsequently separated over silica into neutral and fatty acid fractions using chloroform-saturated ammonia and chloroform:acetic acid (100:1 vol/vol), respectively [*Dickson et al.*, 2009]. The neutral fraction was further fractionated over alumina into apolar and polar fractions using Hexane:DCM (9:1 vol/vol) and DCM:MeOH (1:2 vol/vol), respectively. The polar fraction, containing the GDGTs, was dissolved in hexane/isopropanol (99:1, vol/vol) and passed through 0.45 μm PTFE filters. Fractions were analyzed by high-performance liquid chromatography/atmospheric pressure chemical ionization–mass spectrometry (HPLC/APCI-MS) using a ThermoFisher Scientific Accela Quantum Access. Normal phase separation was achieved on an Alltech Prevail Cyano column (150 mm × 2.1 mm; 3 μm i.d.) with a flow rate of 0.2 ml min^{-1}. Initial solvent was hexane/isopropanol 99:1 (vol/vol), eluted isocratically for 5 min, and followed by a linear gradient to 1.8% isopropanol over 45 min. Analyses were performed in selective ion monitoring mode (SIM) to increase sensitivity and reproducibility, and [M+H]$^+$ (protonated molecular ion) GDGT peaks were integrated.

2.3. GDGT-Based SST Indices

To reconstruct SST, *Kim et al.* [2010] invoke two separate TEX$_{86}$-based SST indices and calibrations. TEX$_{86}^H$ uses the same combination of GDGTs as in the original TEX$_{86}$ relationship [*Schouten et al.*, 2002; *Kim et al.*, 2008] and is defined as

$$\text{GDGT index-2} = \log \frac{[\text{GDGT-2}] + [\text{GDGT-3}] + [\text{Cren.}']}{[\text{GDGT-1}] + [\text{GDGT-2}] + [\text{GDGT-3}] + [\text{Cren.}']} \tag{1}$$

where numbers refer to individual GDGT structures shown in Figure 2. GDGT index-2 is correlated to SST using the calibration equation:

$$\text{TEX}_{86}^H\text{-derived SST} = 68.4 \times (\text{GDGT index-2}) + 38.6 \text{ [calibration error: } \pm 2.5°C] \tag{2}$$
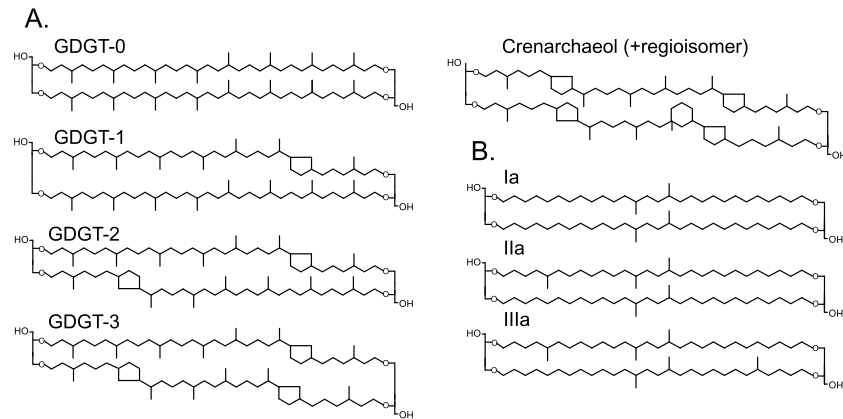
Figure 2. (a) Isoprenoidal and (b) branched glycerol dialkyl glycerol tetraethers used to calculate TEX_{86} and related indices.

TEX_{86}^L employs a combination of GDGTs that is different from TEX_{86}^H, removing GDGT-3 from the numerator and excluding crenarchaeol regioisomer (Cren.') entirely:

$$\text{GDGT index-1} = \log \frac{[\text{GDGT-2}]}{[\text{GDGT-1}] + [\text{GDGT-2}] + [\text{GDGT-3}]} \qquad (3)$$

GDGT index-1 is correlated to SST using the calibration equation:

$$TEX_{86}^L\text{-derived SST} = 67.5 \times (\text{GDGT index-1}) + 46.9 \, [\text{calibration error: } \pm 4°C] \qquad (4)$$

Kim et al. [2010] argue that TEX_{86}^L can be used to reconstruct SST across all temperature ranges, whereas TEX_{86}^H is restricted to SST reconstruction above 15°C. Above 15°C, TEX_{86}^H has a smaller standard calibration error, but both calibrations should yield similar temperatures and no significant offset should exist between them in the modern ocean (ΔH-L = 0) [*Taylor et al.*, 2013]. Despite this, unexpectedly large ΔH-L offsets exist during the Eocene [e.g., *Hollis et al.*, 2012]. *Hollis et al.* [2012] also observed that Eocene TEX_{86}^H SSTs are higher than those derived from inorganic proxies (i.e., Mg/Ca ratios and δ^{18}O values for planktic foraminifera). As a result, *Hollis et al.* [2012] developed an Eocene or "paleo" calibration based on the relationship between these inorganic SST proxies and GDGT ratio-2:

$$\text{SST} = 39.036^*(\text{GDGT-ratio 2}) + 36.455 \, (r^2 = 0.87) \qquad (5)$$

This relationship (defined as pTEX_{86}) [*Hollis et al.*, 2012] is derived from four Eocene records in which TEX_{86} indices and SSTs based on well-preserved, mixed layer planktic foraminifera have been determined for the same samples [*Zachos et al.*, 2006; *Pearson et al.*, 2007; *Burgess et al.*, 2008; *Hollis et al.*, 2009]. In the SW Pacific, this yields SST estimates that are consistently lower than TEX_{86}^H but are generally similar to those derived using TEX_{86}^L [*Hollis et al.*, 2012]. *Taylor et al.* [2013] argue that the ΔH-L offset is a function of the GDGT-2/GDGT-3 ratio ([2]/[3] ratio). As this ratio is markedly higher in deeper waters than the mixed layer [*Taylor et al.*, 2013], it is governed by export dynamics [*Hernández-Sánchez et al.*, 2014] but also partly related to water depth. For example, deep settings (>1000 m) in the modern ocean are characterized by low ΔH-L offsets (<3.0) and high [2]/[3] ratios (>5.0), whereas shallow settings (<1000 m) are characterized by high ΔH-L values (>3.0) and low [2]/[3] ratios (<5.0). Other recent developments in TEX_{86} palaeothermometry include the expansion of the core-top data set into subpolar and polar regions [*Ho et al.*, 2014] and the development of a spatially varying, TEX_{86} Bayesian regression model (BAYSPAR) [*Tierney and Tingley*, 2014]. In deep-time settings, BAYSPAR searches the modern core-top data set for TEX_{86} values which are similar to the measured TEX_{86} value and draws regression parameters from these modern "analogue" locations. SSTs are derived using an online graphical use interface (GUI) (www.whoi.edu/bayspar) [*Tierney and Tingley*, 2014]. Using this approach, an Eocene high-latitude site will draw analogues from a modern-day midlatitude site and so on. However, BAYSPAR does not resolve the problem of high ΔH-L offsets, as the SSTs tend to be similar to those derived from TEX_{86}^H [*Tierney and Tingley*, 2014]. This is not surprising as BAYSPAR is based upon the original TEX_{86} ratio.

2.4. Other GDGT-Based Indices

A number of indices have been developed to screen for potential secondary influences on TEX_{86}. The ratio of branched GDGTs to crenarchaeol (Figure 2) in marine and lacustrine sediments is a function of terrestrial input, expressed as the Branched versus Isoprenoid Tetraether (BIT) index:

$$BIT = \frac{Ia + IIa + IIIa}{Ia + IIa + IIIa + [Crenarchaeol]} \qquad (6)$$

Numbers refer to individual GDGT structures shown in Figure 2. It has been argued that TEX_{86} estimates with BIT values >0.3 should not be used for SST reconstruction due to the potential influence of soil-derived GDGTs on temperature estimates [*Weijers et al.*, 2006b]. Although the BIT has been applied within deep-time settings [*Sluijs et al.*, 2011; *Jenkyns et al.*, 2012], it is unclear whether a threshold of 0.3 remains applicable.

The Methane Index (MI) was proposed to distinguish the relative input of methanotrophic Euryarchaeota versus ammonia-oxidizing Thaumarchaeota in settings characterized by gas-hydrate-related anaerobic oxidation of methane (AOM) [*Pancost et al.*, 2001; *Wakeham et al.*, 2003; *Stadnitskaia et al.*, 2008; *Y. G. Zhang et al.*, 2011]:

$$MI = \left(\frac{[GDGT-1] + [GDGT-2] + [GDGT-3]}{[GDGT-1] + [GDGT-2] + [GDGT-3] + [Crenarchaeol] + [Cren.']} \right) \qquad (7)$$

High MIs (>0.5) reflect high rates of gas-hydrate-related AOM and low values (<0.3) suggest normal sedimentary conditions (i.e., no appreciable AOM input); by extension, TEX_{86} values should be excluded when MI values > 0.5.

Sedimentary archaeal methanogens can synthesize GDGT-0, as well as smaller quantities of GDGT-1, GDGT-2, and GDGT-3 [*Koga et al.*, 1993; *Weijers et al.*, 2006a]. The %GDGT-0 index can be used to qualitatively evaluate the contribution of methanogenic archaea to the sedimentary GDGT pool:

$$\%GDGT\text{-}0 = ([GDGT\text{-}0]/([GDGT\text{-}0] + [Crenarchaeol]))*100 \qquad (8)$$

%GDGT-0 values from thaumarchaeotal enrichment cultures fall below 67%, such that an additional, potentially methanogenic, source of GDGT-0 is likely when %GDGT-0 values exceed this threshold. *Blaga et al.* [2009] and *Sinninghe Damsté et al.* [2012] argue that TEX_{86} values become unreliable in lacustrine settings when %GDGT-0 values >67%, possibly because such a large methanogen input also contributes additional GDGT-1, GDGT-2, and GDGT-3 that can bias TEX_{86} values. However, it is unclear if a similar threshold applies to marine sediments.

2.5. Statistical Analysis

During the Eocene, TEX_{86} SST records have different sampling densities and/or span different intervals [*Pearson et al.*, 2007; *Burgess et al.*, 2008; *Bijl et al.*, 2009; *Hollis et al.*, 2009; *Liu et al.*, 2009; *Hollis et al.*, 2012; *Bijl et al.*, 2013]. To address this problem, time series which spanned the majority of the investigated time window (i.e., ODP 925, ODP 929, ODP 913, ODP 1172, IODP 1356, TDP, SDB, Mid-Waipara, and Hampden Beach) were grouped into low- (<30°) or high-latitude (>55°) bins. Using TEX_{86}^{H} each time series was then turned into a relative temperature (ΔT) by comparison to the warmest temperature in that time series. In order to determine the long-term mean SST evolution in each bin (high and low latitudes) with an associated uncertainty, separate nonparametric LOESS regressions were fitted to both the low- and high-latitude TEX_{86}^{H} ΔSST compilations using the R software package (http://www.R-project.org/). The degree of smoothing (i.e., the span term) was optimized for each time series using generalized cross validation, and an uncertainty envelope (±95% confidence intervals) was calculated based upon the observed scatter of data around the best fit line. Sequential removal of one time series at a time (jackknifing) was also performed to examine the influence of each record on the long-term mean SST (see supporting information).

2.6. Modeling Setup

HadCM3L, a modified version of the UKMO Unified Model HadCM3 [*Gordon et al.*, 2000] fully coupled Atmosphere-Ocean General Circulation model (AOGCM), was employed within this study. The atmospheric and oceanic components of the model comprise a resolution of 2.5° by 3.75°, with 19 vertical levels in the atmosphere and 20 vertical levels in the ocean. Four time slice simulations were constructed utilizing high-
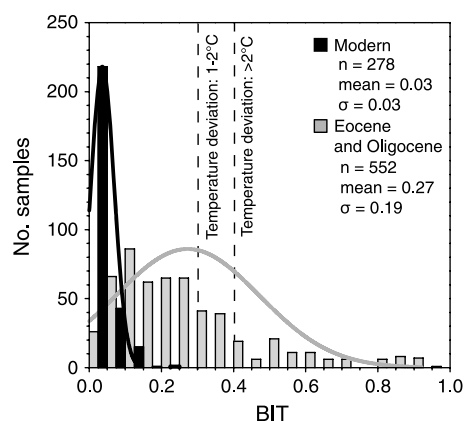
Figure 3. Histogram of BIT indices from open-marine core-top sediments (black) [*Schouten et al.*, 2013] and Eocene and Oligocene sediments (grey bars). Line represents the normal distribution curve for modern and Eocene and Oligocene BIT indices.

resolution paleogeographic boundary conditions under the framework of *Markwick and Valdes* [2004] representing the Ypresian (56.0–47.8 Ma), Lutetian (47.8–41.3 Ma), Bartonian (41.3–38.0 Ma), and Priabonian (38.0–33.9 Ma) geological stages and run for 1422 model years in total to allow surface conditions to approach equilibrium, reducing the error from model drift relative to shorter simulations (see Figure S5). Mean climate state is produced from the final 50 years of the simulation. Following an initial 50 years at 280 ppmv, atmospheric CO_2 is prescribed at 1120 ppmv (4× preindustrial level) for each simulation and with an appropriate solar constant [*Gough*, 1981] representative of each geologic stage defined. The initial ~500 years of the model simulations have a purely baroclinic ocean circulation to ensure stability during spin-up; the barotropic circulation is initialized after 500 years. The barotropic solver in the ocean model requires the definition of continental islands, around which the net ocean flow is nonzero; the defined islands in the model are shown in Figure S6. Note that Antarctica has not been defined as an island in any of these simulations, resulting in a net ocean flow of zero around the margins of Antarctica, even though the palaeogeographic reconstruction implies a possible pathway for circum-Antarctic transport. Due to the small latitudinal extent and shallow depth of the Drake's and Tasman gateways at this time, we do not expect this to greatly affect our results. More details of the climate model itself are described in *Loptson et al.* [2014]; their simulation 4×DYN is carried out with an identical model to the one used here.

3. Results and Discussion

For each site, including new and previously published data sets, we have determined TEX_{86} SSTs during the Eocene and the Oligocene. All of these data sets are described in detail within the supporting information. Using a combination of parameters (BIT, MI, %GDGT-0), we investigate the sedimentary GDGT distributions and discard samples that are potentially problematic with respect to those prospective criteria (see sections 3–5 and supporting information). We then compare ΔH-L offsets against [2]/[3] ratios to explore the applicability of TEX_{86}^{L} before investigating spatial patterns of cooling during the Eocene (see section 6). Based upon our findings, we also reinvestigate cooling trends during the EOT (see section 7).

3.1. Impact of Terrestrial Input Upon Eocene TEX_{86} Values

The observation that branched GDGTs occur predominantly in soils whereas crenarchaeol occurs predominantly in the marine environment led to the development of the branched-to-isoprenoidal tetraether (BIT) index [*Hopmans et al.*, 2004]. Although this was originally used to elucidate the relative input of terrestrial organic matter into the marine realm, it can also provide insights into the efficacy of TEX_{86} estimates [*Hopmans et al.*, 2004; *Weijers et al.*, 2006b; *Fietz et al.*, 2011]. *Weijers et al.* [2006b] show that when BIT values exceed 0.2–0.3, temperature estimates are ~1°C higher than expected, and when BIT values exceed 0.4, temperature estimates can be >2°C higher. However, those observations are specific to that depositional system (the Congo Fan), and the impact of terrigenous GDGTs on reconstructed SST will depend on the nature and temperature of the source catchment. Using our Eocene and Oligocene compilation, we examine the apparent effect of terrestrial input upon TEX_{86} SST estimates.

BIT values from the modern core-top data set do not exceed 0.25 in marine settings [*Schouten et al.*, 2013], with average values of 0.03 (*n* = 278; *σ* = 0.03) (Figure 3). In the Eocene and Oligocene, BIT values associated with TEX_{86} data are higher with an average of 0.27 (*n* = 552; *σ* = 0.19) (Figure 3), likely arising from the fact that many of the Eocene sites from which TEX_{86} records are derived are proximal to land. Many of these proximal settings, such as Tanzania and Seymour Island (Figure 1), do exhibit large temperature deviations (>5°C) when BIT indices are > 0.4 [*Pearson et al.*, 2007; *Douglas et al.*, 2014]. *Sluijs et al.* [2006] suggested that enhanced terrestrial input of GDGT-3 preceding the PETM at IODP Site 302
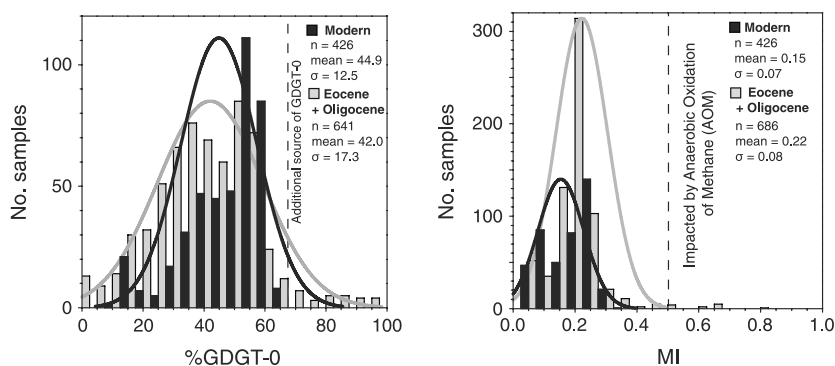
Figure 4. Histogram of (left) %GDGT-0 and (right) MI values from the core-top data set (black) [*Trommer et al.*, 2009; *Kim et al.*, 2010] and Eocene and Oligocene sediments (grey bars). Line represents the normal distribution curve for modern and Eocene and Oligocene %GDGT-0 and MI indices.

(ACEX; Figure 1) resulted in a significant temperature deviation. They removed GDGT-3 from the original TEX$_{86}$ and developed a new index (TEX$_{86}$′) which was calibrated to the modern core-top data set [*Sluijs et al.*, 2006, 2009]. However, we suggest that elevated GDGT-3 is not the only impact of terrigenous OM inputs on isoprenoidal GDGT distributions; i.e., an increase in GDGT-3 due to terrestrial input will also be associated with an increase in the abundance of other isoprenoidal GDGTs. As a result, we argue that TEX$_{86}$′ is not a reliable alternative to SST reconstruction when terrestrial input is high.

TEX$_{86}$ SST estimates from some deep (e.g., ODP Site 929 and ODP Site 925) and shallow (e.g., South Dover Bridge) water settings are relatively unaffected by enhanced terrestrial input. Intriguingly, the few sediment samples from those sites with high BIT values (>0.4) generally yield similar SSTs as those with low BIT values (<0.1). This could be fortuitous, with terrigenous input not causing significant deviations from marine distributions, but it does suggest that the threshold of 0.4 is conservative in some settings.

3.2. Impact of Archaeal Methanogenesis and Methanotrophy Upon Eocene TEX$_{86}$ Values

Considerable work has suggested that sedimentary GDGT production can affect TEX$_{86}$ values and subsequent climate interpretation [*Blaga et al.*, 2009; *Y. G. Zhang et al.*, 2011; *Weijers et al.*, 2011]. Anaerobic methane oxidizing Euryarchaeota, which synthesize isoprenoidal GDGTs containing 0–3 cyclopentane moieties [e.g., *Pancost et al.*, 2001], can affect TEX$_{86}$ values at active cold seeps [*Pancost et al.*, 2001; *Y. G. Zhang et al.*, 2011] and possibly in sediments characterized by diffusive methane flux [*Aquilina et al.*, 2010; *Weijers et al.*, 2011]. Methanogenic archaea, which synthesize small quantities of GDGT-1, GDGT-2, and GDGT-3 [*Koga et al.*, 1993; *Weijers et al.*, 2006b], are also present in marine sediments. Currently, there is no evidence that they impact marine TEX$_{86}$ values although they do appear to affect lacustrine TEX$_{86}$ values [*Blaga et al.*, 2009; *Powers et al.*, 2010; *Sinninghe Damsté et al.*, 2012].

Figure 4a shows %GDGT-0 values for the modern core-top data set and our Eocene compilation. In the modern core-top data set, %GDGT-0 values span a broad range (9–65%, $n = 426$) with an average of 45% ($\sigma = 12.5$). This is expected for core-top sediments unlikely to have been affected by methane cycling [*Martens and Berner*, 1974]. Higher values occur in deeper sediments [*Pancost et al.*, 2008; *Blaga et al.*, 2009] and are associated with the occurrence of ^{13}C-depleted acyclic biphytanes (δ^{13}C: −21‰ to −26‰) (note that depleted relative to thaumarchaeal-derived biphytanes (δ^{13}C: −20‰ to −22‰)) [*Schouten et al.*, 1998; *Pancost et al.*, 2008]. This indicates that GDGT-0 is likely derived from methanogens in deeper horizons. Eocene %GDGT-0 values span a larger range (5 to 97; $n = 641$), although the average %GDGT-0 value is similar to that observed in modern core-top sediments (42%; $\sigma = 17$) (Figure 4a). The majority of samples (>90%) fall below 67%, suggesting that methanogenic contributions are also relatively minor during the Eocene. In modern surface sediments, %GDGT-0 exhibits a positive correlation with latitude ($r^2 = 0.87$) and TEX$_{86}$^{H}-derived SST ($r^2 = 0.55$). Despite some uncertainties in the accuracy of palaeolatitude estimates [e.g., *Self-Trail et al.*, 2012], Eocene %GDGT-0 values exhibit a weaker correlation with latitude ($r^2 = 0.43$) and TEX$_{86}$^{H}-derived SST ($r^2 = 0.36$). This suggests an additional, potentially methanogenic, source of GDGT-0 in older sediments and provides further justification for the exclusion of GDGT-0 in TEX$_{86}$

palaeothermometry [*Schouten et al.*, 2002]. However, the actual impact on Eocene reconstructed temperatures appears to be minor. Only 7% of the Eocene data set yields %GDGT-0 values in excess of 67%, suggesting the presence of an additional, potentially methanogenic, source of GDGT-0. Some of these samples (i.e., ODP Site 913) also contain 2,6,10,15,19-pentamethylicosane (PMI), a common methanogen [*Brassell et al.*, 1981; *Schouten et al.*, 1997] and anaerobic methanotroph biomarker [*Thiel et al.*, 2001], and provide independent evidence for methane cycling at this site.

Several sedimentary sequences contain rather variable %GDGT-0 values, sometimes in adjacent sediments (e.g., Ceara Rise), perhaps as a result of localized bioturbation. In those cases, samples with high %GDGT-0 values do not yield significantly ($<2°C$) different temperature estimates than samples with lower %GDGT-0 values. This suggests that sedimentary methanogenesis does not impact TEX_{86} SST estimates. This contrasts with observations made in lacustrine settings [*Blaga et al.*, 2009; *Sinninghe Damsté et al.*, 2012]. We suggest this is because GDGT-0 and GDGT-1, and possibly GDGT-2 and GDGT-3, co-occur in terrestrial settings [*Pancost and Sinninghe Damsté*, 2003; *Weijers et al.*, 2006a; *Huguet et al.*, 2010], whereas the production of GDGT-0 by methanogens in marine settings is not associated with significant production of GDGT-1 or GDGT-2 (or any other GDGTs used in the TEX_{86} palaeothermometer).

In the modern core-top data set, the Methane Index (MI) spans a narrow range (0.03–0.23) and averages 0.15 ($n = 426$; $\sigma = 0.07$) (Figure 4b). MIs exceed 0.3 in $<$ 1% of samples and do not exceed 0.5. As with %GDGT-0 values, this is expected for core-top sediments which are likely unaffected by methane cycling [*Martens and Berner*, 1974]. In gas-hydrate-impacted and/or methane-rich environments, MIs are higher (>0.6) and span a larger range (~0.6–1.0). In such settings, high MIs are associated with the presence of ^{13}C-depleted biphytanes, providing further evidence for a methanotrophic source [*Wakeham et al.*, 2003; *Wakeham et al.*, 2004; *Bouloubassi et al.*, 2006; *Pancost et al.*, 2008; *Y. G. Zhang et al.*, 2011]. Elevated MIs also occur in older sediments of continental marginal settings characterized by high sedimentation rate and organic matter flux [*Aquilina et al.*, 2010; *Weijers et al.*, 2011]. MIs span a larger range (0.08–0.82) in our Eocene and Oligocene data set (Figure 4b; $n = 686$) and yield a slightly higher average value (0.22; $\sigma = 0.08$) than modern core-top sediments. MIs exceed 0.3 in $\sim$8% of samples and exceed 0.5 in $<$2% of samples, suggesting that most Eocene and Oligocene sediments, despite their continental margin locations, are relatively unaffected by diffusive methane flux and associated anaerobic oxidation of methane.

In the Eocene and Oligocene data set, a nonlinear, positive correlation exists between MI and %GDGT-0 (Figure S1). This is expected because sediment profiles characterized by methanogenesis will likely also have experienced some amount of anaerobic oxidation of methane [*Sivan et al.*, 2007]. This relationship is almost certainly driven by methane cycling rather than temperature, because the latter—by decreasing % GDGT-0 and increasing MIs—would yield a negative rather than positive correlation.

4. Red Sea-Type GDGT Distributions

In the modern core-top calibration, sediments from the Red Sea yield much warmer TEX_{86} SST estimates than observed values [*Trommer et al.*, 2009; *Ionescu et al.*, 2009] and are excluded from the global core-top calibration data sets of *Kim et al.* [2008] and *Kim et al.* [2010] but not the BAYSPAR calibration data set of *Tierney and Tingley* [2014]. Red Sea GDGT distributions are characterized by a low fractional abundance of GDGT-0 relative to Crenarchaeol regioisomer (Cren.′). To identify a typical Red Sea-type distribution within the geological record, we propose the following ratio:

$$\%GDGT_{RS} = ([Cren.']/([GDGT\text{-}0] + [Cren.']))*100 \tag{9}$$

However, we propose this only as an approximate evaluation tool, because other factors, such as temperature [*Schouten et al.*, 2002; *Kim et al.*, 2010], can affect %GDGT$_{RS}$ indices (see later). Thus, we suggest it is initially employed to identify sediments with unusually low amounts of GDGT-0 relative to crenarchaeol regioisomer. Further evaluation of a putative Red Sea-type GDGT signature can be based on the entirety of the GDGT distribution [*Trommer et al.*, 2009].

%GDGT$_{RS}$ values from the modern core-top data set ($n = 396$) [*Kim et al.*, 2010] do not exceed 24, except for the Red Sea, where values range from 32 to 59 ($n = 30$; Figure S2) [*Trommer et al.*, 2009]. As such, we propose hat a Red Sea-type contribution should be considered for %GDGT$_{RS}$ $>$30. In our Eocene compilation, these
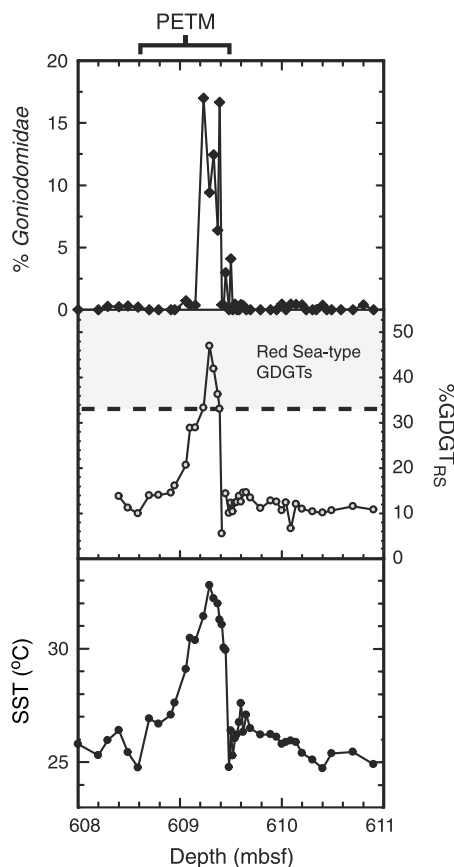
Figure 5. Changes in temperature and salinity across the PETM at ODP Site 1172. (a) SST derived from TEX_{86}^H. (b) $\%GDGT_{RS}$ values. (c) The percentage of *Goniodomoidae*, a hypersaline dinocyst [*Sluijs et al.*, 2011]. Grey area denotes a Red Sea-type GDGT distribution.

thigh $\%GDGT_{RS}$ values are common, widespread and range up to 70. During the Bartonian (41.3–38.0 Ma) and Priabonian (38.0–33.9 Ma), high $\%GDGT_{RS}$ values are confined to low-latitude sites (i.e., Tanzania). There, $\%GDGT_{RS}$ values are highly variable and exhibit no correlation with TEX_{86}^H SSTs. High $\%GDGT_{RS}$ values are especially common during times of elevated warmth (Figure S4). During the Early Eocene Climatic Optimum (EECO), high $\%GDGT_{RS}$ values become more geographically widespread, occurring at ODP Site 1172 [*Bijl et al.*, 2009], Mid-Waipara [*Hollis et al.*, 2009, 2012], Hampden Beach (this paper), and South Dover Bridge (this paper). At these sites, $\%GDGT_{RS}$ values gradually increase during the EECO, attain highest values during peak EECO warmth, and then gradually decrease following the EECO (Figure S4). Similarly, $\%GDGT_{RS}$ values increase at the onset of the PETM at Wilson Lake [*Zachos et al.*, 2006; *Sluijs et al.*, 2007], ODP Site 1172 [*Sluijs et al.*, 2011] (Figure 5), and South Dover Bridge (this paper). GDGT-0 was not detected at Bass River [*Sluijs et al.*, 2007; *Sluijs and Brinkhuis*, 2009]. Unfortunately, it appears that most of the Red Sea GDGT characteristics are indistinguishable from those expected for temperatures in excess of ~30°C (based on projecting correlations to temperatures beyond the modern limits). Therefore, we cannot currently untangle these effects on GDGT distributions in the sedimentary record.

Aside from temperature, the underlying ecological controls that govern the occurrence of these distributions remain unclear. At ODP Site 1172, the dinocyst genus *Eocladopyxis*, a member of the extant family Goniodomidae that mainly inhabits low-latitude lagoonal environments, peaks during the PETM and the EECO [*Sluijs et al.*, 2011] (Figure 5). A peak in *Eocladopyxis* spp. also occurs prior to and immediately after the onset of the PETM at Bass River and Wilson Lake [*Sluijs and Brinkhuis*, 2009]. At all three sites, the occurrence of hypersaline dinocysts coincides with an increase in $\%GDGT_{RS}$ values. The presence of *Eocladopyxis* in the Recent has been explained by hyperstratification and the development of lagoonal conditions in the open ocean [*Reichart et al.*, 2004; *Sluijs and Brinkhuis*, 2009]. At Mid-Waipara River, the dinocyst genus *Homotryblium*, a similar "lagoonal" indicator genus, is also present in low abundances during the early Eocene [*Hollis et al.*, 2009] while other high-salinity, lagoonal dinocysts, such as *Heteraulacacysta* and *Polysphaeidium*, are identified during the PETM at Bass River and Wilson Lake [*Sluijs and Brinkhuis*, 2009]. Although the presence of hypersaline and/or lagoonal dinocysts is consistent with an increase in salinity, they rarely dominate the dinocyst assemblage [e.g., *Sluijs et al.*, 2011] and it is possible that other factors exert a control upon Red Sea-type GDGT distributions.

Pure cultures of *Nitrosopumilis Maritimus*, a marine group I.1a thaumarchaeon, indicate that nutrient availability can influence GDGT distributions [*Elling et al.*, 2014]. However, this contrasts with *Trommer et al.* [2009] who correlated Red Sea TEX_{86} values with nitrate concentrations at 100 m depth and found no obvious correlation. Alternatively, *Kim et al.* [2015] argue that modern Red Sea GDGT distributions originate from a deep-water (>1000 m) thaumarchaeotal community. Using core-top sediments from the Mediterranean and the Red Sea, *Kim et al.* [2015] recently developed a regional TEX_{86} SST calibration for deep-water (>1000 m), restricted basins. This yields lower TEX_{86} SSTs, both in the modern and during the Eocene. However, as Eocene Red Sea-type GDGT distributions are restricted to shallow water settings (typically <500 m), this calibration is deemed unsuitable here.
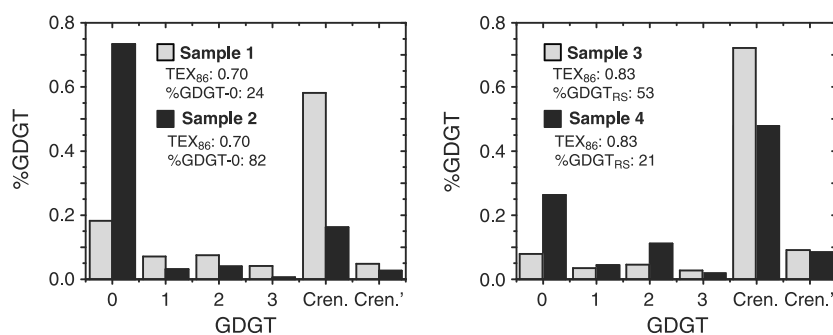
Figure 6. Interrogating GDGT distributions. Samples derived from (1) Mid-Waipara River, (2) ODP Site 929, (3) ODP Site 925, and (4) Hampden Beach.

Intriguingly, high %$GDGT_{RS}$ values and Red Sea-like GDGT distributions also occur in Mesozoic sediments, including in Oceanic Anoxic Event 1b sediments deposited at ODP Site 1049 [*Kuypers et al.*, 2001; *Kuypers et al.*, 2002]. There, a range of biomarker evidence has shown that deposition of organic-rich sediments represents an unusual and widespread expansion of archaea [*Kuypers et al.*, 2002]. The most diagnostic biomarkers for OAE1b archaeal assemblages, i.e., tetramethylicosane (TMI), have not been reported for the Eocene sediments discussed here nor the Red Sea. This could provide additional evidence for extreme Palaeogene and Mesozoic warmth; i.e., they reflect additional changes in the GDGT distribution beyond those reflected by TEX_{86} values. Alternatively, they could reflect the same factors that influence Red Sea distributions and that overestimate SST. As Red Sea GDGT characteristics are indistinguishable from those expected for temperatures in excess of ~30°C; we continue to include high %$GDGT_{RS}$ values within our long-term Eocene compilation.

5. Interrogating GDGT Distributions

BIT, %GDGT-0, MI, and %$GDGT_{RS}$ are useful tools which can be used to flag potentially problematic TEX_{86} values. However, there are limitations to a single numerical representation of these complex GDGT distributions. Figure 6a shows two sets of Eocene GDGT distributions with identical TEX_{86} values (0.70). Sample 2 has a much higher %GDGT-0 value than Sample 1 and suggests an additional, potentially methanogenic, source of isoprenoidal GDGTs. Otherwise, the GDGT distribution is very similar to Sample 1 and suggests the SST reconstructions are valid. In Figure 6b, Samples 3 and 4 also have identical TEX_{86} values (0.83) but different %$GDGT_{RS}$ values, Sample 4 being characterized by a Red Sea-type GDGT distribution. As Red Sea-type GDGT distributions fall off the core-top calibration line for $TEX_{86}{}^{H}$ [*Schouten et al.*, 2002; *Kim et al.*, 2010], this sample from Hampden Beach could overestimate SST (see section 4).

This translation of a complex GDGT distribution into a single TEX_{86} value can also be problematic for the BAYSPAR approach. BAYSPAR searches the modern core-top data set for TEX_{86} values that are similar to the measured TEX_{86} value and draws regression parameters from these modern "analogue" locations. When a TEX_{86} value exceeds 0.75, BAYSPAR typically draws regression parameters from the modern-day Red Sea. This assumes the ancient GDGT distribution is similar to the modern-day Red Sea; however, there are a number of Eocene and Oligocene localities where high TEX_{86} values (>0.75) are not characterized by a Red Sea-type GDGT distribution (e.g., ODP 628, ODP 803, and ODP Site 925). In these samples, the Red Sea is an inappropriate analogue for a warm, subtropical site [*Tierney and Tingley*, 2014] and highlights the need to investigate the entire GDGT distribution before reconstructing SST.

6. Descent Toward the Icehouse

6.1. Comparison of GDGT-Based SST Proxies for the Eocene

The following section focuses upon SST estimates derived using $TEX_{86}{}^{H}$, $TEX_{86}{}^{L}$ and $pTEX_{86}$ (see later). However, there are a number of other TEX_{86} calibrations which merit further discussion. The current mesocosm calibration extends to 40°C [*Wuchter et al.*, 2004; *Kim et al.*, 2010] and may be preferable in low-

latitude "greenhouse" environments. However, in mesocosm studies, the fractional abundance of the crenarchaeol isomer is ~14 fold lower than expected and we thus argue against applying this calibration in deep-time settings. The application of a linear [*Schouten et al.*, 2002; *Tierney and Tingley*, 2014], logarithmic [*Kim et al.*, 2010] or reciprocal [*Liu et al.*, 2009] calibration will also impact SST reconstructions, particularly in low-latitude greenhouse environments. However, the linear calibration yields unrealistically high SST values (>30℃) during the Holocene [*Kim et al.*, 2010], and we therefore argue against its application in modern and ancient (sub)tropical climates. BAYSPAR, which also utilizes a linear calibration, does not appear to yield unrealistically high SST values during the Quaternary [e.g., *Tierney and Tingley*, 2014]; however, it does not formally addresses regional/oceanographic variations in deeper time reconstructions. This is because the analogue is generated by sampling within TEX_{86} space (as discussed in section 2.3) rather than on the basis of oceanographic (productivity regime) or regional (water depth, circulation, seasonal) considerations. The reciprocal approach [*Liu et al.*, 2009], which yields similar SST estimates as the logarithmic approach [*Kim et al.*, 2010], is associated with a maximum temperature of 35℃ and is therefore also unsuitable for low-latitude greenhouse environments.

TEX_{86}^{L}- and TEX_{86}^{H}-based temperature offsets (ΔH-L), both today and in the Paleogene, are similar in deep (>1000 m) water settings but up to 10℃ different in shallow (<1000 m) settings, suggesting that the choice of proxy is crucial in the latter setting [*Taylor et al.*, 2013]. ΔH-L offsets are a function of the GDGT-2/GDGT-3 ([2]/[3]) ratio, such that high ΔH-L offsets correspond to low [2]/[3] ratios and vice versa. Sedimentary [2]/[3] ratios appear to be elevated when there is a greater contribution of subsurface GDGTs to the sedimentary GDGT pool [*Taylor et al.*, 2013; *Kim et al.*, 2015]. After discarding TEX_{86} values with potentially problematic GDGT distributions (as discussed above and shown in the supporting information), we use [2]/[3] ratios and ΔH-L offsets [*Taylor et al.*, 2013] to evaluate the various TEX_{86} calibrations for each site.

In the SW Pacific (ODP Site 1172, IODP Site 1356, Mid-Waipara River, and Hampden Beach; Figure 1), high ΔH-L offsets and low [2]/[3] ratios are consistent with sediments deposited in a relatively shallow water setting. It has been shown that the lower TEX_{86}^{L}-derived SSTs are similar to inorganic and modeled SST estimates [*Hollis et al.*, 2012; *Bijl et al.*, 2013]. TEX_{86}^{L}-derived SSTs exhibit a stronger latitudinal temperature gradient (~10℃) than TEX_{86}^{H}, which yields much warmer SW Pacific SSTs (~27–33℃) and a low-latitudinal SST gradient. $pTEX_{86}$, which has been calibrated to inorganic proxies, gives SW Pacific temperatures similar to those of TEX_{86}^{L}. All three calibrations exhibit a similar timing and magnitude of cooling through the Eocene [*Bijl et al.*, 2009; *Hollis et al.*, 2012; *Bijl et al.*, 2013]. In the South Atlantic (Seymour Island; Figure 1), [2]/[3] ratios and ΔH-L offsets are also consistent with sediments deposited in a relatively shallow water setting. There, SSTs derived from inorganic proxies, in this case clumped isotope paleothermometry, are similar to TEX_{86}^{L}-derived SSTs but colder than TEX_{86}^{H} [*Douglas et al.*, 2014].

In the North Atlantic (ODP Site 913; Figure 1), TEX_{86}^{H} and TEX_{86}^{L} yield similar SSTs, consistent with sediments deposited in a deeper water setting [*Myhre et al.*, 1995; *Eldrett et al.*, 2004]. In contrast, SST estimates derived from $pTEX_{86}$ are significantly colder. In the western tropical Atlantic (ODP Site 925, ODP Site 929; Figure 1), in a relatively open ocean setting, [2]/[3] ratios are high and ΔH-L offsets are low, consistent with sediments deposited in a deep-water setting (>1000 m). TEX_{86}^{H} and TEX_{86}^{L} all indicate late Eocene cooling, but the magnitude of cooling in TEX_{86}^{L} is much larger than expected (~7℃). Moreover, $pTEX_{86}$ and TEX_{86}^{L} SSTs are colder than expected for a tropical location (21–28℃).

In the Indian Ocean (Tanzania; Figure 1), [2]/[3] ratios are low and ΔH-L offsets are high; however, there is wide scatter in Tanzania TEX_{86}^{L} values when compared with inorganic SST estimates, and the overall correlation to SST derived from foraminiferal $\delta^{18}O$ values is stronger when TEX_{86}^{H} is employed [*Hollis et al.*, 2012]. Overall, the distributions of GDGTs in Eocene sediments agree with previous findings that shallow water settings are associated with large ΔH-L offsets and small [2]/[3] ratios, and vice versa. However, there are exceptions, including Lomonosov Ridge (ACEX) and ODP Site 511 (Figure 1), which are both shallow water settings with relatively small ΔH-L offsets. This reinforces previous arguments that water depth is not the primary control on differences between TEX_{86}^{H} and TEX_{86}^{L}-derived SSTs [*Taylor et al.*, 2013; *Kim et al.*, 2015]. Instead, we argue that differences are controlled by the magnitude of the subsurface GDGT contribution to sediments, which can be related to water depth but is also governed by the range of factors related to export productivity [*Hernández-Sánchez et al.*, 2014].

Our data also challenge the simple framework that TEX_{86}^L is most applicable in shallow water settings. In the Atlantic (South Dover Bridge; Figure 1) and Gulf Coastal Plain [*Keating-Bitonti et al.*, 2011], [2]/[3] ratios and ΔH-L offsets are consistent with samples deposited in a shallow setting. However, TEX_{86}^L SST estimates are unexpectedly low for a subtropical setting (22°C) and are, in fact, 2–3°C colder than contemporary SST estimates [*Levitus and Boyer*, 1994]. A similar problem has been observed in the Gulf of Mexico Coastal Plain during the late Paleocene (~15°C) and PETM (~25°C) [*Sluijs et al.*, 2013]. At Hampden Beach, [2]/[3] ratios and ΔH-L offsets are consistent with samples deposited in a shallow setting. However, there are large variations in TEX_{86}^L SST estimates which are inconsistent with inorganic and organic SST estimates from nearby sites [*Bijl et al.*, 2009; *Hollis et al.*, 2009; *Creech et al.*, 2010; *Hollis et al.*, 2012; *Bijl et al.*, 2013]. These estimates may reflect local variations in SST; alternatively, they may be related to the TEX_{86}^L index which is far more sensitive to contributions from other archaea and, in particular, the fractional abundance of GDGT-3.

Thus, although TEX_{86}^L does agree with inorganic proxies in some shallow water settings [*Hollis et al.*, 2009; *Hollis et al.*, 2012; *Douglas et al.*, 2014], there are exceptions. Modern water column investigations suggest that the TEX_{86}^L calibration should be used with great caution. Recently, *Taylor et al.* [2013] showed that the increase in [2]/[3] ratios with depth is a globally widespread feature of GDGT distributions in the water column, possibly due to the predominance of different Thaumarchaeota communities in the surface mixed layer and subsurface [*Villanueva et al.*, 2014]. The implication is that subsurface export has a markedly stronger impact on TEX_{86}^L values than on TEX_{86}^H and, by extension, that the depth-related difference between TEX_{86}^L- and TEX_{86}^H-derived SSTs is due to complexities associated with the former. As a result, the following section is restricted to the discussion of TEX_{86}^H-derived SSTs.

6.2. Sea Surface Temperature Change During the Eocene

Present-day SST rarely exceeds 28–29°C (except in some isolated basins), which some have suggested indicates a homeostatic limit to tropical SST [*Ramanathan and Collins*, 1991; *Kleypas et al.*, 2008]. This has however been shown to be ill-founded [*Pierrehumbert*, 1995; *van Hooidonk and Huber*, 2009; *Williams et al.*, 2009] and is not supported by SST records in the more recent geological past [*O'Brien et al.*, 2014]. During the early and middle Eocene, SST estimates from Tanzania [*Pearson et al.*, 2007], Ceara Rise (ODP Site 925; ODP Site 929) [*Liu et al.*, 2009] and the Atlantic Coastal Plain (South Dover Bridge) regularly exceed this modern limit, with TEX_{86}^H-derived SSTs > 32°C (Figure 7). TEX_{86}^H SSTs, which are clearly higher than those of today, do not support the existence of a tropical "thermostat" [*O'Brien et al.*, 2014; *Pagani*, 2014], at least insofar as it is most strictly defined [*Ramanathan and Collins*, 1991].

Previous work stipulated that if SSTs were truly ~35°C in Tanzania [*Pearson et al.*, 2007], then some tropical regions (e.g., the Western Pacific Warm Pool (WPWP) must have been much hotter [*Huber*, 2008]. Indeed, our modeling simulations indicate that the WPMP (~34°C) was ~3–4°C warmer than Tanzania (~30–31°C) (Figure 10). Moderately higher tropical temperatures relative to today (>2°C) will significantly increase evaporation rates, latent heat transport [*Huber and Sloan*, 2000], and the frequency and/or the strength of tropical cyclones [*Sriver and Huber*, 2007]. Tropical cyclones help to induce ocean mixing which enhances meridional overturning and ocean heat transport. This can reduce the latitudinal temperature gradient by up to 6°C and warm high-latitude oceans by as much as 10°C [*Sriver and Huber*, 2007; *Thomas et al.*, 2014].

Our record also suggests tropical cooling during the Eocene, albeit of much lesser magnitude than that observed at high southern latitudes [see later; *Bijl et al.*, 2009; *Hollis et al.*, 2009; *Creech et al.*, 2010; *Hollis et al.*, 2012; *Bijl et al.*, 2013]. TEX_{86}^H indicates ≤2°C of tropical cooling within the Indian Ocean during the middle and late Eocene (45–34 Ma; Figure 8), 3–4°C of cooling within the western equatorial Atlantic during the middle and late Eocene (40–34 Ma; Figure 8), and 4–5°C of cooling within the subtropical Atlantic Coastal Plain between the early and middle Eocene (53–41 Ma; Figure 8). Crucially, middle and late Eocene (47.8–34.0 Ma) tropical cooling is apparent regardless of the calibration. By fitting a nonparametric LOESS regression to our compiled data set, we are able to determine that there was ~2.5°C of long-term tropical surface water cooling between the early and late Eocene (Figure 9b) Jackknifing (the sequential removal of one record at a time) revealed that no single time series overly influences the magnitude of Eocene cooling determined by LOESS regression; however, removal of the South Dover Bridge record does change the pattern of the low-latitude long-term cooling (Figure S7). Slight tropical cooling, as indicated by TEX_{86}^H, remains consistent with inorganic $\delta^{18}O$ evidence from Tanzania which
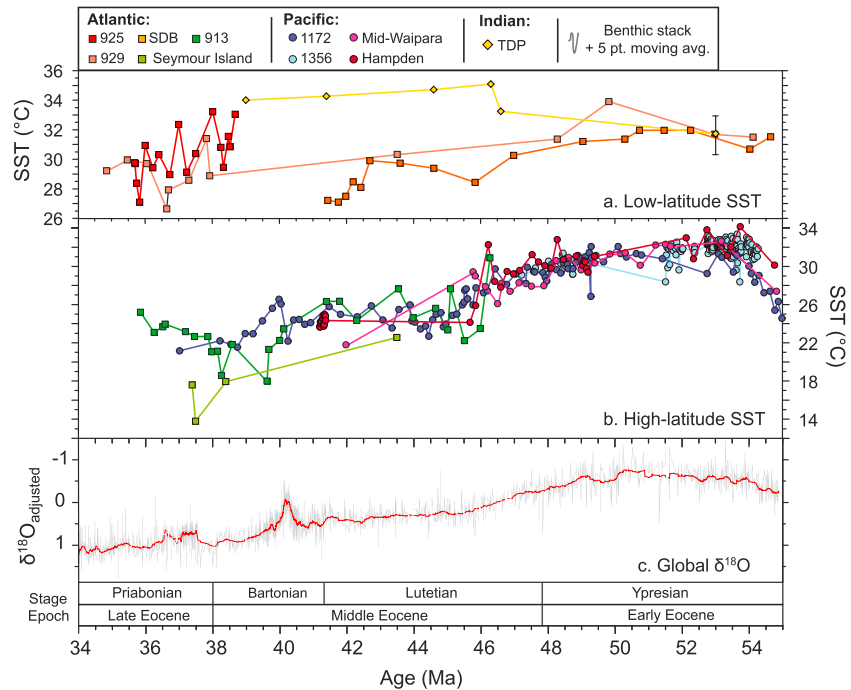
Figure 7. Absolute TEX$_{86}^{H}$ SST record during the Eocene (55–34 Ma). (a) Low-latitude TEX$_{86}^{H}$ SSTs, (b) high-latitude TEX$_{86}^{H}$ SSTs, and (c) global benthic foraminiferal δ^{18}O stack (updated to GTS2012) in grey with red being the 30 point moving average [*Cramer et al.*, 2011]. Error bars on TEX$_{86}^{H}$ are 2.5°C. Filled squares, diamonds, and circles reflect SST estimates from the Atlantic, Indian Ocean, and the SW Pacific, respectively.

suggests slightly cooler temperatures, perhaps coupled with increasing ice volume, in the late Eocene and early Oligocene [*Pearson et al.*, 2007].

For comparison, a nonparametric LOESS regression was fitted through the compiled high-latitude data set. This approach indicates ~6°C of high-latitude cooling between the early and late Eocene (Figure 9c). As with the low-latitude compilation, jackknifing revealed that no single record influences the overall magnitude of long-term high-latitude cooling determined by LOESS regression (Figure S8). However, because the IODP 1356 time series has a very high sampling density around the EECO, its removal causes the general cross validation optimization routine to choose a relatively low degree of smoothing, such that the long-term mean high-latitude SST determined without this record exhibits more structure in the Mid and Late Eocene (Figure S8). Nonetheless, long-term average high-latitude cooling, as indicated by TEX$_{86}^{H}$ (and also BAYSPAR), is also in agreement with inorganic Mg/Ca SST estimates [*Creech et al.*, 2010; *Hollis et al.*, 2012] and δ^{18}O BWT estimates [*Cramer et al.*, 2011] which indicate amplified polar cooling during the Eocene epoch.

6.3. Latitudinal SST Gradients During the Eocene

Our revised SST compilation provides new insights into global cooling during the descent toward the icehouse. During the early Eocene (56.0–47.8 Ma), the temperature difference (ΔT) between the tropics (2.5–4.5°N) and the SW Pacific (~55–65°) is very low (ΔT: <2°C) (Figure 7) when compared with modern conditions, as has been extensively noted and discussed elsewhere [*Bijl et al.*, 2009; *Hollis et al.*, 2009; *Hollis et al.*, 2012]. Gradual cooling in the SW Pacific during the middle Eocene (47.8–38.0 Ma) progressively strengthens the southern hemisphere SST gradient (Figure 7). During the late Eocene (38.0–33.9 Ma), the latitudinal SST gradient between the SW Pacific (ODP Site 1772) and the tropics is markedly stronger than the early Eocene (ΔT: ~9°C) (Figure 7) but remains much smaller than observed today (ΔT: >25°C) [*Douglas et al.*, 2014].

During the late middle Eocene (41.3–38.0 Ma), the temperature difference between the equatorial Atlantic (2.5–4.5°N) and the South Atlantic (52–67°S) is relatively large (ΔT: 14°C) (Figure 7). Although there is cooling in the South Atlantic during the middle late and late Eocene, the latitudinal temperature gradient
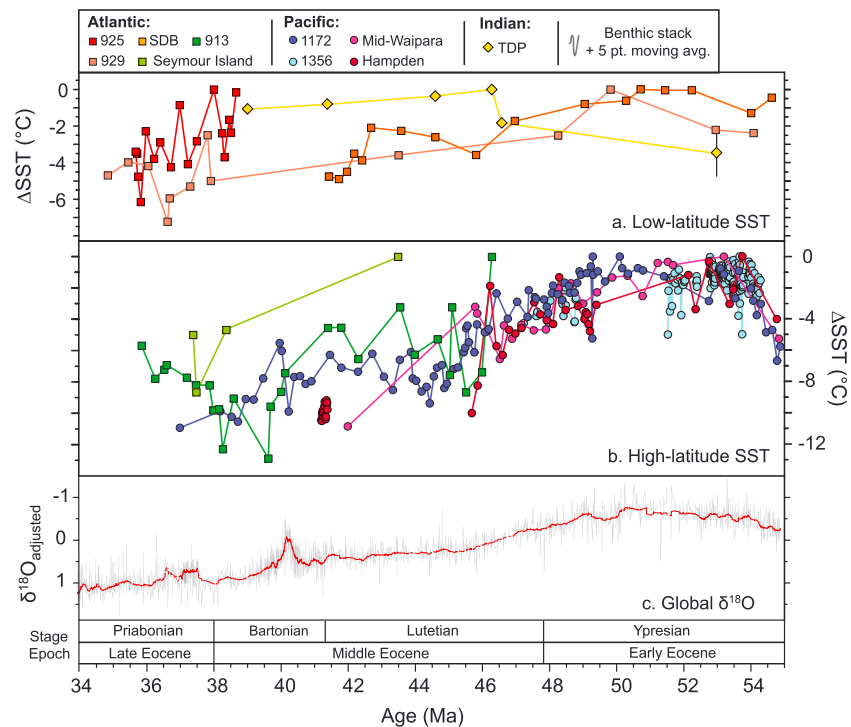
Figure 8. Normalized TEX_{86}^H SST record during the Eocene (55–34 Ma). (a) Low-latitude TEX_{86}^H SSTs, (b) high-latitude TEX_{86}^H SSTs, and (c) global benthic foraminiferal $\delta^{18}O$ stack (updated to GTS2012) in grey with red being the 30 point moving average [*Cramer et al.*, 2011]. Error bars on TEX_{86}^H are 2.5°C. Filled squares, diamonds, and circles reflect SST estimates from the Atlantic, Indian Ocean, and the SW Pacific, respectively.

between the equatorial and South Atlantic weakens during this interval (ΔT: 12°C) as a result of tropical cooling (Figures 7 and 8).

During the early middle Eocene (47.8–41.3 Ma), the temperature difference between the equatorial Atlantic (2.5–4.5°N) and the North Atlantic (67°N) is also low (ΔT: 5°C) (Figure 7) and similar to the temperature difference between the SW Pacific and the tropics (ΔT: 5°C). Analogous to the SW Pacific, there is no strong cooling trend in the North Atlantic during the early middle Eocene (Figure 7). Immediately following the MECO (~40 Ma), the latitudinal SST gradient strengthens (ΔT: ~14°C) (Figure 7) before weakening during the late middle and late Eocene (38.0–33.9 Ma) (ΔT: ~5°C).

Previous studies have shown that latitudinal temperature gradients of less than 20°C are difficult for climate models to simulate and require large changes in latitudinal heat transport and/or substantial positive feedbacks acting at high latitudes [*Huber and Sloan*, 1999; *Bice et al.*, 2000; *Huber et al.*, 2003; *Lunt et al.*, 2012]. As a result, the application of TEX_{86}^H in high-latitude sites cannot be reconciled with modeled SSTs during the early Eocene [*Hollis et al.*, 2012; *Sijp et al.*, 2014]. However, a closer agreement between proxies and models can be obtained via changes in the physical parameters of the model (e.g., cloud cover) [*Sagoo et al.*, 2013].

6.4. Assessing the Driving Mechanisms: CO_2, Gateways, or Both?

The apparent tropical SST stability observed by *Pearson et al.* [2007] suggests that mechanisms such as gateway reorganization [*Sijp et al.*, 2011] may have been important in regulating high-latitude cooling during the Eocene [*Bijl et al.*, 2009, 2013]. However, we note that *Pearson et al.* [2007] never argued that tropical SSTs were constant during the Eocene, only that SST change was much smaller than inferred from the oxygen isotopic composition of diagenetically altered foraminifera [*Bralower et al.*, 1995; *Dutton et al.*, 2005]. In fact, a small cooling trend (perhaps coupled with minor ice growth) is apparent in the well-preserved foraminifera in Tanzanian sediments during the middle Eocene (47.8–38.0 Ma) [*Pearson et al.*, 2007]. Although this is not reflected in the original low-resolution Tanzanian TEX_{86} data, our new higher-resolution TEX_{86} data (Figures 7 and 8) and compiled tropical SST record fitted with a nonparametric LOESS regression (Figure 9) indicate the tropics cooled during the middle and late Eocene (47.8–34.0 Ma).
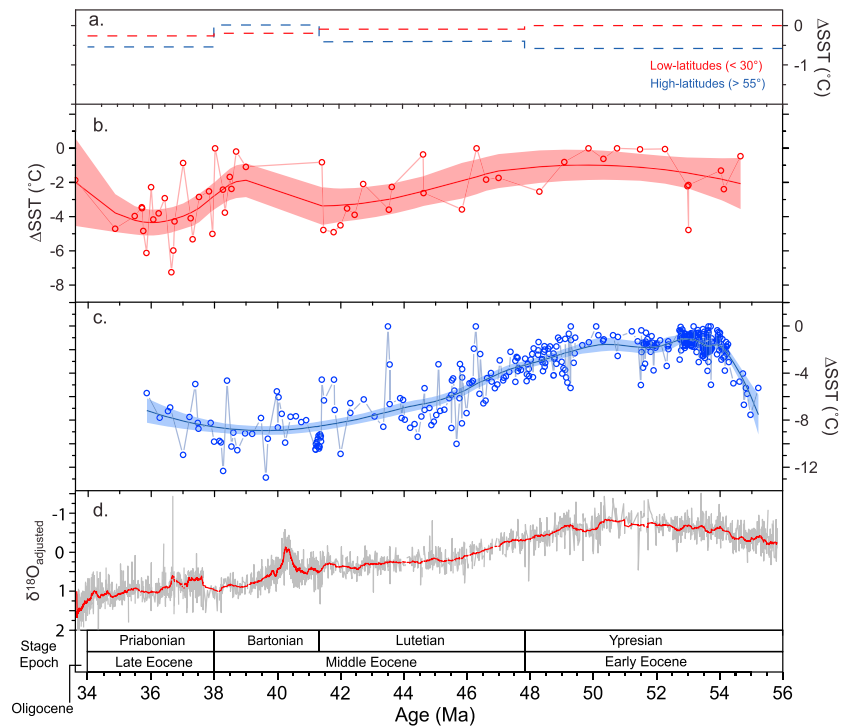
Figure 9. Temperature change during the Eocene (55–34 Ma). (a) HadCM3L model output of SST for low (<30°) and high latitudes (>55°) during each stage of the Eocene. Atmospheric CO_2 is prescribed at 1120 ppmv (4× preindustrial level). (b) Normalized, low-latitude (red) TEX_{86}^H SSTs fitted with a nonparametric LOESS regression. Band reflects the area within which 68% of the data lie. (c) Normalized, high-latitude (blue) TEX_{86}^H SSTs fitted with a nonparametric LOESS regression. Band reflects the area within which 68% of the data lie. (d) Global benthic foraminiferal $\delta^{18}O$ stack in grey (updated to GTS2012) with red being the 30 point moving average [*Cramer et al.*, 2011].

To examine the influence of gateway reorganization upon tropical cooling, we have generated corresponding model-derived SST estimates during each geological Stage of the Eocene using the HadCM3L model (section 2.6; Figures 10, S5 and S6; Tables S2 and S3). The model simulations all have a fixed atmospheric CO_2 concentration of 4× preindustrial values (i.e., 1120 ppmv), and the difference in solar constant between the simulation is relatively small. As such, any temperature variation between the simulations should record the role of ocean gateway reorganization and palaeogeographic change upon global ocean circulation. In our model simulations, the Tasman Gateway is closed during the Ypresian (47.8–56 Ma) with early opening during the Lutetian (41.3–47.8 Ma) and significant deepening during the Priabonian (33.9–38.0 Ma), in agreement with proxy evidence [*Stickley et al.*, 2004; *Bijl et al.*, 2013] (Figure 10). The Drake Passage (DP) is open throughout the Ypresian and Lutetian (Figure 10), in contrast with tectonic and geochemical evidence which suggests that the DP remained closed until the early Bartonian (~41 Ma) [*Scher and Martin*, 2006; *Livermore et al.*, 2007; *Borrelli et al.*, 2014]. Despite this the total rate of transport (1.3–3 Sverdrups (Sv); Table S1) across the DP during the Ypresian and the Lutetian simulations is very small when compared to modern observations (~130 Sv) [*Chidichimo et al.*, 2014]. The Tethys Ocean remains open between the Ypresian (47.8–56.0 Ma) and the Priabonian (33.9–38.0 Ma) (Figure 10), in line with tectonic evidence [*McQuarrie et al.*, 2003; *Allen and Armstrong*, 2008].

Our constant-pCO_2 model simulations indicate that on a regional scale, low-latitude (<30°) SSTs decrease by ~0.3°C between the early and late Eocene (Figure 9a). During the same interval, compiled, proxy-derived SSTs decrease by 2.5°C (Figure 9b). Based upon this, and assuming the model and boundary conditions are not fundamentally flawed, changes in gateways and palaeogeography can only account for ~10% of the low-latitude, proxy-derived cooling between the early and late Eocene. Although the magnitude of model-derived SST change varies on a site-by-site basis (see Tables S2 and S3), our results indicate that oceanographic change related to palaeogeographic change cannot account for the majority of tropical cooling.
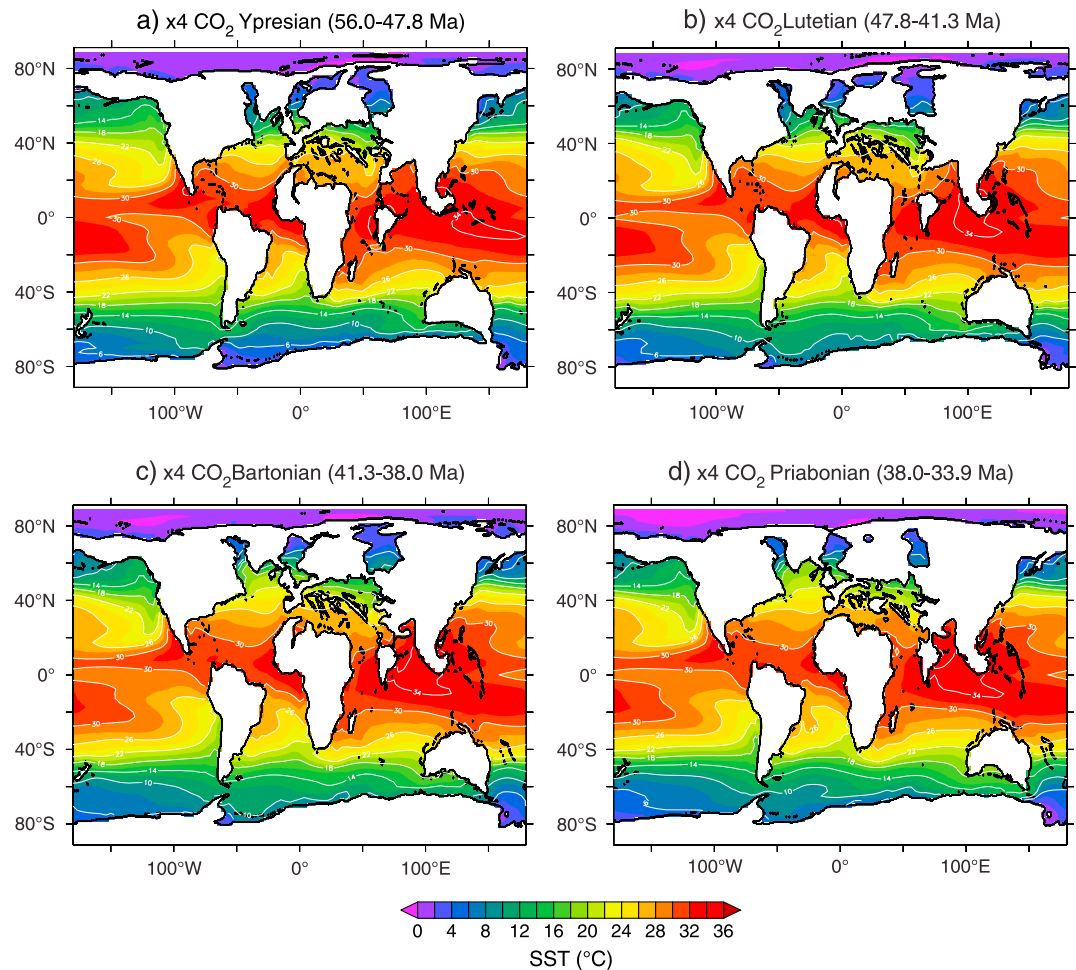
Figure 10. Model-derived SST estimates from four time slice simulations representing the Ypresian (56.0–47.8 Ma), Lutetian (47.8–41.3 Ma), Bartonian (41.3–38.0 Ma), and Priabonian (38.0–33.9 Ma) geological stages. Atmospheric CO_2 is prescribed at 1120 ppmv (4× preindustrial level).

Bathymetric change (such as gateway openings) may have been responsible for other specific regional features. For example, *Sijp et al.* [2009] argue that opening the DP can account for ~5°C of Antarctic cooling under modern-day bathymetries. However, later studies, using inferred Eocene bathymetry, indicate that the magnitude of Antarctic cooling associated with DP opening is negligible (<0.5°C) [*Zhang et al.*, 2010; *Z. Zhang et al.*, 2011; *Lefebvre et al.*, 2012; *Goldner et al.*, 2014]. *Bijl et al.* [2013] argue that initial deepening of the Tasman Gateway ~49–50 Ma coincided with westward throughflow of the proto–Antarctic Circumpolar Current (ACC), resulting in surface water and continental cooling in the SW Pacific and along the East Antarctic margin [*Pross et al.*, 2012; *Bijl et al.*, 2013]. Evidence from neodymium isotopes [*Scher and Martin*, 2006], clumped isotope, and TEX_{86} paleothermometry [*Bijl et al.*, 2009; *Douglas et al.*, 2014] and model simulations of intermediate complexity [*Sijp et al.*, 2014] also indicate that initial opening of the Tasman Gateway is linked to the intensification of deep-water formation in the Ross Sea [*Bijl et al.*, 2014]. Our model simulations indicate that on a regional scale, high-latitude (>55°) SSTs increase by ~0.4°C between the early and late Eocene (Figure 9a). During the same interval, compiled, high-latitude proxy-derived SSTs decrease by ~6°C (Figure 9b). Based upon this, changes in paleogeography cannot account for the observed high-latitude, proxy-derived cooling during the Eocene (Tables S2–S4). On a local scale, high-latitude, HadCM3L-derived SSTs remain relatively stable (e.g., at the site of ACEX, 913) or increase during the Eocene (e.g., at the site of 1172, Hampden, 1356) (Table S3), indicating that changes in paleogeography are unable to explain the entirety of high-latitude cooling and that other mechanisms, such as CO_2 drawdown, must be invoked. However, it should be noted that models often struggle to

replicate specific oceanographic features. For example, the subtropical East Antarctic Current (EAC) may have extended as far south as ~54° during the early Eocene and could have been responsible for warming the surface waters of ODP Site 1172 and New Zealand [*Hollis et al.*, 2012]. In contrast, many models struggle to replicate this phenomena [e.g., *Lunt et al.*, 2012, and references therein]. HadCM3L also exhibits a relatively strong early Eocene latitudinal SST gradient compared to other models (e.g., ECHAM5 or CCSM3) [*Lunt et al.*, 2012], in contradiction to several lines of evidence from proxies [e.g., *Bijl et al.*, 2009].

The evolution of $p\mathrm{CO}_2$ during the Eocene remains poorly constrained, particularly during the early Eocene [*Beerling et al.*, 2011; *Hyland and Sheldon*, 2013]. Using TEX_{86} and an ensemble of climate model simulations which span the Eocene, we conclude that the some portion of tropical cooling (~10%) can be explained by changes in paleogeography and/or ocean gateways. However, the majority of high-latitude cooling cannot be explained by changes in ocean gateways and, in the absence of other plausible forcing mechanisms, indicates that CO_2 was primarily responsible for global surface water cooling during the Eocene.

7. Descent Into the Icehouse

Long-term gradual cooling during the Eocene culminated in the establishment of permanent ice sheets on the Antarctic continent in the earliest Oligocene. This relatively rapid ice sheet expansion may have been driven by southern ocean gateway opening [*Katz et al.*, 2008, 2011], declining $p\mathrm{CO}_2$ concentrations [*DeConto and Pollard*, 2003; *Pearson et al.*, 2009; *Pagani et al.*, 2011], or a combination of the two. During this interval, tropical TEX_{86} SST estimates decrease by up to 13°C [*Liu et al.*, 2009]. However, these values are hard to reconcile with Mg/Ca SST estimates [*Lear et al.*, 2008] and $\mathrm{U}^{K'}_{37}$ SST estimates [*Liu et al.*, 2009]. This suggests that parameters other than SST are controlling TEX_{86} values during the EOT. Based upon our earlier discussion, we reinvestigate this possibility using the TEX_{86}^{H} proxy.

From the latest Eocene (~34–37 Ma) into the earliest Oligocene (~33–34 Ma), low-latitude TEX_{86}^{H} SST estimates decrease, on average, between 0.2 and 5.6°C. However, this does not take into account the full range of cooling which can exceed 10°C within tropical ODP Sites 998 and 803. Both sites are characterized by very high [2]/[3] ratios and low-to-negative ΔH-L offsets, suggesting the presence of "deep-water" Thaumarchaeota throughout the late Eocene and early Oligocene [*Taylor et al.*, 2013; *Kim et al.*, 2015]. As deep-water GDGTs can be incorporated into the sedimentary GDGT pool [e.g., *Kim et al.*, 2015], this could account for some of the observed temperature change in tropical settings across the EOT. The intensification of Antarctic bottom water formation and enhanced equatorward transport of Antarctic intermediate water associated with Antarctic glaciation [*Katz et al.*, 2011; *Goldner et al.*, 2014] could have also influenced the depth of GDGT production during this interval. It certainly could have impacted the depth of and temperature change across the tropical thermocline, both of which could have impacted subsurface GDGT production, export, and recorded temperature. Other tropical settings, such as ODP 925 and ODP 929, are characterized by relatively modest cooling (~3°C) and do not appear to be affected by changes in deep-water export of GDGTs. Future studies should attempt to exploit depositional settings which are less likely to be affected by deep-water GDGT export.

8. Conclusions

Using new and previously published GDGT distributions, we have generated a composite TEX_{86} SST record for the Eocene (55–34 Ma). To investigate the influence of archaea other than marine Thaumarchaeota upon Eocene (and Oligocene) TEX_{86} values, we compiled and compared BIT indices, MIs, and %GDGT-0 values from modern and ancient sediments. Our results indicate that Eocene and Oligocene sediments have similar average values as the modern core-top data set but larger standard deviations. Nonetheless, it appears that the effect of archaea other than marine Thaumarchaeota upon Eocene and Oligocene TEX_{86} values is minimal. Our compiled TEX_{86} compilation indicates that between the early and late Eocene, high-latitudes SSTs cooled by ~6°C and low-latitudes SST cooled by ~2.5°C. Global sea surface cooling during the Eocene is not in agreement with by fixed-CO_2 HadCM3L model simulations. Therefore, our study provides indirect evidence that drawdown of CO_2 (or some, as of yet unidentified, other factor(s)) was the primary forcing for long-term climatic cooling during the Eocene. Our data set, combined with forthcoming model simulations under a range of different CO_2 levels, paves the way to reconstructing atmospheric CO_2 evolution through the Eocene.

References

Allen, M. B., and H. A. Armstrong (2008), Arabia–Eurasia collision and the forcing of mid-Cenozoic global cooling, *Palaeogeogr. Palaeoclimatol. Palaeoecol.*, *265*(1–2), 52–58.

Aquilina, A., N. Knab, K. Knittel, G. Kaur, A. Geissler, S. Kelly, H. Fossing, C. Boot, R. Parkes, and R. Mills (2010), Biomarker indicators for anaerobic oxidizers of methane in brackish-marine sediments with diffusive methane fluxes, *Org. Geochem.*, *41*(4), 414–426.

Beerling, D. J., A. Fox, D. S. Stevenson, and P. J. Valdes (2011), Enhanced chemistry-climate feedbacks in past greenhouse worlds, *Proc. Natl. Acad. Sci. U.S.A.*, *108*, 9770–9775.

Bice, K. L., C. R. Scotese, D. Seidov, and E. J. Barron (2000), Quantifying the role of geographic change in Cenozoic ocean heat transport using uncoupled atmosphere and ocean models, *Palaeogeogr. Palaeoclimatol. Palaeoecol.*, *161*(3–4), 295–310.

Bijl, P. K., S. Schouten, A. Sluijs, G.-J. Reichart, J. C. Zachos, and H. Brinkhuis (2009), Early Palaeogene temperature evolution of the southwest Pacific Ocean, *Nature*, *461*(7265), 776–779.

Bijl, P. K., et al. (2013), Eocene cooling linked to early flow across the Tasmanian Gateway, *Proc. Natl. Acad. Sci. U.S.A.*, *110*(24), 9645–9650.

Blaga, C. I., G.-J. Reichart, O. Heiri, and J. S. S. Damsté (2009), Tetraether membrane lipid distributions in water-column particulate matter and sediments: A study of 47 European lakes along a north–south transect, *J. Paleolimnol.*, *41*(3), 523–540.

Borrelli, C., B. S. Cramer, and M. E. Katz (2014), Bipolar Atlantic deepwater circulation in the middle-late Eocene: Effects of Southern Ocean gateway openings, *Paleoceanography*, *29*, 308–327, doi:10.1002/2012PA002444.

Bouloubassi, I., G. Aloisi, R. D. Pancost, E. Hopmans, C. Pierre, and J. S. Sinninghe Damsté (2006), Archaeal and bacterial lipids in authigenic carbonate crusts from eastern Mediterranean mud volcanoes, *Org. Geochem.*, *37*(4), 484–500.

Bralower, T. J., J. C. Zachos, E. Thomas, M. Parrow, C. K. Paull, D. C. Kelly, I. P. Silva, W. V. Sliter, and K. C. Lohmann (1995), Late Paleocene to Eocene paleoceanography of the equatorial Pacific Ocean: Stable isotopes recorded at Ocean Drilling Program Site 865, Allison Guyot, *Paleoceanography*, *10*(4), 841–865, doi:10.1029/95PA01143.

Brassell, S., A. Wardroper, I. Thomson, J. Maxwell, and G. Eglinton (1981), Specific acyclic isoprenoids as biological markers of methanogenic bacteria in marine sediments, *Nature*, *290*, 693–696.

Burgess, C. E., P. N. Pearson, C. H. Lear, H. E. Morgans, L. Handley, R. D. Pancost, and S. Schouten (2008), Middle Eocene climate cyclicity in the southern Pacific: Implications for global ice volume, *Geology*, *36*(8), 651–654.

Chidichimo, M. P., K. A. Donohue, D. R. Watts, and K. L. Tracey (2014), Baroclinic transport time series of the Antarctic Circumpolar Current measured in Drake Passage, *J. Phys. Oceanogr.*, *44*(7), 1829–1853.

Contreras, L., J. Pross, P. K. Bijl, A. Koutsodendris, J. I. Raine, B. van de Schootbrugge, and H. Brinkhuis (2013), Early to Middle Eocene vegetation dynamics at the Wilkes Land Margin (Antarctica), *Rev. Palaeobot. Palynol.*, *197*, 119–142.

Cramer, B., K. Miller, P. Barrett, and J. Wright (2011), Late Cretaceous–Neogene trends in deep ocean temperature and continental ice volume: Reconciling records of benthic foraminiferal geochemistry ($\delta18$O and Mg/Ca) with sea level history, *J. Geophys. Res.*, *116*, C12023, doi:10.1029/2011JC007255.

Creech, J. B., J. A. Baker, C. J. Hollis, H. E. Morgans, and E. G. Smith (2010), Eocene sea temperatures for the mid-latitude southwest Pacific from Mg/Ca ratios in planktonic and benthic foraminifera, *Earth Planet. Sci. Lett.*, *299*(3), 483–495.

DeConto, R. M., and D. Pollard (2003), Rapid Cenozoic glaciation of Antarctica induced by declining atmospheric CO_2, *Nature*, *421*(6920), 245–249.

Dickson, L., I. D. Bull, P. J. Gates, and R. P. Evershed (2009), A simple modification of a silicic acid lipid fractionation protocol to eliminate free fatty acids from glycolipid and phospholipid fractions, *J. Microbiol. Methods*, *78*(3), 249–254.

Douglas, P. M. J., H. P. Affek, L. C. Ivany, A. J. P. Houben, W. P. Sijp, A. Sluijs, S. Schouten, and M. Pagani (2014), Pronounced zonal heterogeneity in Eocene southern high-latitude sea surface temperatures, *Proc. Natl. Acad. Sci. U.S.A.*, *111*(18), 6582–6587.

Dutton, A., K. C. Lohmann, and R. M. Leckie (2005), Insights from the Paleogene tropical Pacific: Foraminiferal stable isotope and elemental results from Site 1209, Shatsky Rise, *Paleoceanography*, *20*, PA3004, doi:10.1029/2004PA001098.

Eder, W., M. Schmidt, M. Koch, D. Garbe-Schönberg, and R. Huber (2002), Prokaryotic phylogenetic diversity and corresponding geochemical data of the brine–seawater interface of the Shaban Deep, Red Sea, *Environ. Microbiol.*, *4*(11), 758–763.

Eldrett, J. S., I. C. Harding, J. V. Firth, and A. P. Roberts (2004), Magnetostratigraphic calibration of Eocene–Oligocene dinoflagellate cyst biostratigraphy from the Norwegian–Greenland Sea, *Mar. Geol.*, *204*(1), 91–127.

Elling, F. J., M. Könneke, J. S. Lipp, K. W. Becker, E. J. Gagen, and K.-U. Hinrichs (2014), Effects of growth phase on the membrane lipid composition of the thaumarchaeon Nitrosopumilus maritimus and their implications for archaeal lipid distributions in the marine environment, *Geochim. Cosmochim. Acta*, *141*, 579–597.

Fietz, S., A. Martínez-Garcia, C. Huguet, G. Rueda, and A. Rosell-Melé (2011), Constraints in the application of the Branched and Isoprenoid Tetraether index as a terrestrial input proxy, *J. Geophys. Res.*, *116*, C10032, doi:10.1029/2011JC007062.

Francis, J. E., and I. Poole (2002), Cretaceous and early Tertiary climates of Antarctica: Evidence from fossil wood, *Palaeogeogr. Palaeoclimatol. Palaeoecol.*, *182*(1–2), 47–64.

Goldner, A., N. Herold, and M. Huber (2014), Antarctic glaciation caused ocean circulation changes at the Eocene-Oligocene transition, *Nature*, *511*(7511), 574–577.

Gordon, C., C. Cooper, C. A. Senior, H. Banks, J. M. Gregory, T. C. Johns, J. F. B. Mitchell, and R. A. Wood (2000), The simulation of SST, sea ice extents and ocean heat transports in a version of the Hadley Centre coupled model without flux adjustments, *Clim. Dyn.*, *16*(2–3), 147–168.

Gough, D. (1981), Solar interior structure and luminosity variations, in *Physics of Solar Variations*, vol. 74, pp. 21–34, Springer, Netherlands.

Gradstein, F. M., G. Ogg, and M. Schmitz (2012), *The Geologic Time Scale 2012 2-Volume Set*, pp. 92, Elsevier, Amsterdam.

Hernández-Sánchez, M., E. Woodward, K. Taylor, G. Henderson, and R. Pancost (2014), Variations in GDGT distributions through the water column in the South East Atlantic Ocean, *Geochim. Cosmochim. Acta*, *132*, 337–348.

Ho, S. L., Mollenhauer, G., Fietz, S., Martínez-Garcia, A., Lamy, F., Rueda, G., Schipper, K., Méheust, M., Rosell-Melé, A., and Stein, R. (2014), Appraisal of TEX$_{86}$ and thermometries in subpolar and polar regions, *Geochim. Cosmochim. Acta*, *131*, 213–226, doi:10.1016/j.gca.2014.01.001.

Hollis, C. J., L. Handley, E. M. Crouch, H. E. Morgans, J. A. Baker, J. Creech, K. S. Collins, S. J. Gibbs, M. Huber, and S. Schouten (2009), Tropical sea temperatures in the high-latitude South Pacific during the Eocene, *Geology*, *37*(2), 99–102.

Hollis, C. J., et al. (2012), Early Paleogene temperature history of the Southwest Pacific Ocean: Reconciling proxies and models, *Earth Planet. Sci. Lett.*, *349–350*, 53–66.

Hopmans, E. C., J. W. Weijers, E. Schefuß, L. Herfort, J. S. Sinninghe Damsté, and S. Schouten (2004), A novel proxy for terrestrial organic matter in sediments based on branched and isoprenoid tetraether lipids, *Earth Planet. Sci. Lett.*, *224*(1), 107–116.

Huber, M. (2008), Climate change. A Hotter Greenhouse?, *Science*, *321*, 353.

Huber, M., and L. C. Sloan (1999), Warm climate transitions: A general circulation modeling study of the late Paleocene thermal maximum (~56 Ma), *J. Geophys. Res.*, *104*(D14), 16,633–16,655, doi:10.1029/1999JD900272.

Huber, M., and L. C. Sloan (2000), Climatic responses to tropical sea surface temperature changes on a "greenhouse" Earth, *Paleoceanography*, *15*(4), 443–450, doi:10.1029/1999PA000455.

Huber, M., L. C. Sloan, and C. Shellito (2003), Early Paleogene oceans and climate: A fully coupled modeling approach using the NCAR CCSM, *Geol. Soc. Am. Spec. Pap.*, *369*, 25–47.

Huguet, A., C. Fosse, F. Laggoun-Défarge, M.-L. Toussaint, and S. Derenne (2010), Occurrence and distribution of glycerol dialkyl glycerol tetraethers in a French peat bog, *Org. Geochem.*, *41*(6), 559–572.

Hyland, E. G., and N. D. Sheldon (2013), Coupled CO2-climate response during the Early Eocene Climatic Optimum, *Palaeogeogr. Palaeoclimatol. Palaeoecol.*, *369*, 125–135.

Ionescu, D., S. Penno, M. Haimovich, B. Rihtman, A. Goodwin, D. Schwartz, L. Hazanov, M. Chernihovsky, A. F. Post, and A. Oren (2009), Archaea in the Gulf of Aqaba, *FEMS Microbiol. Ecol.*, *69*(3), 425–438.

Jenkyns, H., L. Schouten-Huibers, S. Schouten, and J. Sinninghe Damsté (2012), Warm Middle Jurassic–Early Cretaceous high-latitude sea-surface temperatures from the Southern Ocean, *Clim. Past*, *8*(1), 215–226.

Jurgens, G., K. Lindström, and A. Saano (1997), Novel group within the kingdom Crenarchaeota from boreal forest soil, *Appl. Environ. Microbiol.*, *63*(2), 803–805.

Karner, M. B., E. F. DeLong, and D. M. Karl (2001), Archaeal dominance in the mesopelagic zone of the Pacific Ocean, *Nature*, *409*(6819), 507–510.

Katz, M. E., K. G. Miller, J. D. Wright, B. S. Wade, J. V. Browning, B. S. Cramer, and Y. Rosenthal (2008), Stepwise transition from the Eocene greenhouse to the Oligocene icehouse, *Nat. Geosci.*, *1*(5), 329–334.

Katz, M. E., B. S. Cramer, J. Toggweiler, G. Esmay, C. Liu, K. G. Miller, Y. Rosenthal, B. S. Wade, and J. D. Wright (2011), Impact of Antarctic Circumpolar Current development on late Paleogene ocean structure, *Science*, *332*(6033), 1076–1079.

Kennett, J. P., and N. F. Exon (2004), Paleoceanographic evolution of the Tasmanian Seaway and its climatic implications, in *The Cenozoic Southern Ocean: Tectonics, Sedimentation, and Climate Change Between Australia and Antarctica*, edited by N. F. Exon, J. P. Kennett, and M. J. Malone, pp. 345–367, AGU, Washington, D. C.

Keating-Bitonti, C. R., L. C. Ivany, H. P. Affek, P. Douglas, and S. D. Samson (2011), Warm, not super-hot, temperatures in the early Eocene subtropics, *Geology*, *39*(8), 771–774.

Kim, J.-H., S. Schouten, E. C. Hopmans, B. Donner, and J. S. Sinninghe Damsté (2008), Global sediment core-top calibration of the TEX$_{86}$ paleothermometer in the ocean, *Geochim. Cosmochim. Acta*, *72*(4), 1154–1173.

Kim, J.-H., J. Van der Meer, S. Schouten, P. Helmke, V. Willmott, F. Sangiorgi, N. Koç, E. C. Hopmans, and J. S. S. Damsté (2010), New indices and calibrations derived from the distribution of crenarchaeal isoprenoid tetraether lipids: Implications for past sea surface temperature reconstructions, *Geochim. Cosmochim. Acta*, *74*(16), 4639–4654.

Kim, J.-H., S. Schouten, M. Rodrigo-Gámiz, S. Rampen, G. Marino, C. Huguet, P. Helmke, R. Buscail, E. C. Hopmans, and J. Pross (2015), Influence of deep-water derived isoprenoid tetraether lipids on the paleothermometer in the Mediterranean Sea, *Geochim. Cosmochim. Acta*, *150*, 125–141.

Kleypas, J. A., G. Danabasoglu, and J. M. Lough (2008), Potential role of the ocean thermostat in determining regional differences in coral reef bleaching events, *Geophys. Res. Lett.*, *35*, L03613, doi:10.1029/2007GL032257.

Koga, Y., M. Nishihara, H. Morii, and M. Akagawa-Matsushita (1993), Ether polar lipids of methanogenic bacteria: Structures, comparative aspects, and biosyntheses, *Microbiol. Rev.*, *57*(1), 164–182.

Kuypers, M. M., P. Blokker, J. Erbacher, H. Kinkel, R. D. Pancost, S. Schouten, and J. S. S. Damsté (2001), Massive expansion of marine archaea during a mid-Cretaceous oceanic anoxic event, *Science*, *293*(5527), 92–95.

Kuypers, M. M., Pancost, R. D., Nijenhuis, I. A., and Sinninghe Damsté, J. S. (2002), Enhanced productivity led to increased organic carbon burial in the euxinic North Atlantic basin during the late Cenomanian oceanic anoxic event, *Paleoceanography*, *17*(4), 1051, doi:10.1029/2000PA000569.

Lear, C. H., T. R. Bailey, P. N. Pearson, H. K. Coxall, and Y. Rosenthal (2008), Cooling and ice growth across the Eocene-Oligocene transition, *Geology*, *36*(3), 251–254.

Lefebvre, V., Y. Donnadieu, P. Sepulchre, D. Swingedouw, and Z. S. Zhang (2012), Deciphering the role of southern gateways and carbon dioxide on the onset of the Antarctic Circumpolar Current, *Paleoceanography*, *27*, PA4201, doi:10.1029/2012PA002345.

Levitus, S., and T. P. Boyer (1994), World Ocean Atlas 1994, Volume 4, Temperature, National Environmental Satellite, Data, and Information Service, Washington, D. C.

Liu, Z., M. Pagani, D. Zinniker, R. DeConto, M. Huber, H. Brinkhuis, S. R. Shah, R. M. Leckie, and A. Pearson (2009), Global cooling during the Eocene-Oligocene climate transition, *Science*, *323*(5918), 1187–1190.

Livermore, R., C.-D. Hillenbrand, M. Meredith, and G. Eagles (2007), Drake Passage and Cenozoic climate: An open and shut case?, *Geochem. Geophys. Geosyst.*, *8*, Q01005, doi:10.1029/2005GC001224.

Loptson, C. A., D. J. Lunt, and J. E. Francis (2014), Investigating vegetation-climate feedbacks during the early Eocene, *Clim. Past*, *10*(2), 419–436.

Lowenstein, T. K., and R. V. Demicco (2006), Elevated Eocene atmospheric CO$_2$ and its subsequent decline, *Science*, *313*(5795), 1928–1928.

Lunt, D. J., et al. (2012), A model–data comparison for a multi-model ensemble of early Eocene atmosphere–ocean simulations: EoMIP, *Clim. Past*, *8*(5), 1717–1736.

Martens, C. S., and R. A. Berner (1974), Methane production in the interstitial waters of sulfate-depleted marine sediments, *Science*, *185*(4157), 1167–1169.

Markwick, P. J., and P. J. Valdes (2004), Palaeo-digital elevation models for use as boundary conditions in coupled ocean–atmosphere GCM experiments: A Maastrichtian (late Cretaceous) example, *Palaeogeogr. Palaeoclimatol. Palaeoecol.*, *213*(1–2), 37–63.

McQuarrie, N., Stock, J. M., Verdel, C., and Wernicke, B. P. (2003), Cenozoic evolution of Neotethys and implications for the causes of plate motions, *Geophys. Res. Lett.*, *30*(20), 2036, doi:10.1029/2003GL017992.

Myhre, A., J. Thiede, J. Firth, and Shipboard Scientific Party (1995), North Atlantic-Arctic Gateways I: in *Proceedings Ocean Drilling Program, ODP, Init. Repts.: sites 907–913, 151*, p. 926.

O'Brien, C. L., G. L. Foster, M. A. Martinez-Boti, R. Abell, J. W. B. Rae, and R. D. Pancost (2014), High sea surface temperatures in tropical warm pools during the Pliocene, *Nat. Geosci.*, *7*(8), 606–611.

Ochsenreiter, T., D. Selezi, A. Quaiser, L. Bonch-Osmolovskaya, and C. Schleper (2003), Diversity and abundance of Crenarchaeota in terrestrial habitats studied by 16S RNA surveys and real time PCR, *Environ. Microbiol.*, *5*(9), 787–797.

Pagani, M. (2014), Palaeoclimate: Broken tropical thermostats, *Nat. Geosci.*, *7*(8), 555–556.

Pagani, M., J. C. Zachos, K. H. Freeman, B. Tipple, and S. Bohaty (2005), Marked decline in atmospheric carbon dioxide concentrations during the Paleogene, *Science*, *309*(5734), 600–603.

Pagani, M., M. Huber, Z. Liu, S. M. Bohaty, J. Henderiks, W. Sijp, S. Krishnan, and R. M. DeConto (2011), The role of carbon dioxide during the onset of Antarctic glaciation, *Science*, *334*(6060), 1261–1264.

Pancost, R., E. Hopmans, and J. Sinninghe Damsté (2001), Archaeal lipids in Mediterranean cold seeps: Molecular proxies for anaerobic methane oxidation, *Geochim. Cosmochim. Acta*, *65*(10), 1611–1627.

Pancost, R. D., and J. S. Sinninghe Damsté (2003), Carbon isotopic compositions of prokaryotic lipids as tracers of carbon cycling in diverse settings, *Chem. Geol.*, *195*(1), 29–58.

Pancost, R. D., J. M. Coleman, G. D. Love, A. Chatzi, I. Bouloubassi, and C. E. Snape (2008), Kerogen-bound glycerol dialkyl tetraether lipids released by hydropyrolysis of marine sediments: A bias against incorporation of sedimentary organisms?, *Org. Geochem.*, *39*(9), 1359–1371.

Pearson, A., and A. E. Ingalls (2013), Assessing the use of archaeal lipids as marine environmental proxies, *Annu. Rev. Earth Planet. Sci.*, *41*, 359–384.

Pearson, A., A. P. McNichol, B. C. Benitez-Nelson, J. M. Hayes, and T. I. Eglinton (2001), Origins of lipid biomarkers in Santa Monica Basin surface sediment: A case study using compound-specific $\Delta^{14}C$ analysis, *Geochim. Cosmochim. Acta*, *65*(18), 3123–3137.

Pearson, P. N., and M. R. Palmer (2000), Atmospheric carbon dioxide concentrations over the past 60 million years, *Nature*, *406*(6797), 695–699.

Pearson, P. N., B. E. van Dongen, C. J. Nicholas, R. D. Pancost, S. Schouten, J. M. Singano, and B. S. Wade (2007), Stable warm tropical climate through the Eocene Epoch, *Geology*, *35*(3), 211–214.

Pearson, P. N., G. L. Foster, and B. S. Wade (2009), Atmospheric carbon dioxide through the Eocene–Oligocene climate transition, *Nature*, *461*(7267), 1110–1113.

Pester, M., C. Schleper, and M. Wagner (2011), The Thaumarchaeota: An emerging view of their phylogeny and ecophysiology, *Curr. Opin. Microbiol.*, *14*(3), 300–306.

Pierrehumbert, R. (1995), Thermostats, radiator fins, and the local runaway greenhouse, *J. Atmos. Sci.*, *52*(10), 1784–1806.

Powers, L., J. P. Werne, A. J. Vanderwoude, J. S. Sinninghe Damsté, E. C. Hopmans, and S. Schouten (2010), Applicability and calibration of the TEX$_{86}$ paleothermometer in lakes, *Org. Geochem.*, *41*(4), 404–413.

Pross, J., L. Contreras, P. K. Bijl, D. R. Greenwood, S. M. Bohaty, S. Schouten, J. A. Bendle, U. Röhl, L. Tauxe, and J. I. Raine (2012), Persistent near-tropical warmth on the Antarctic continent during the early Eocene epoch, *Nature*, *488*(7409), 73–77.

Qian, P.-Y., Y. Wang, O. O. Lee, S. C. Lau, J. Yang, F. F. Lafi, A. Al-Suwailem, and T. Y. Wong (2011), Vertical stratification of microbial communities in the Red Sea revealed by 16S rDNA pyrosequencing, *ISME J.*, *5*(3), 507–518.

Ramanathan, V., and W. Collins (1991), Thermodynamic regulation of ocean warming by cirrus clouds deduced from observations of the 1987 El Nino, *Nature*, *351*(6321), 27–32.

Reichart, G. J., H. Brinkhuis, F. Huiskamp, and W. J. Zachariasse (2004), Hyperstratification following glacial overturning events in the northern Arabian Sea, *Paleoceanography*, *19*, PA2013, doi:10.1029/2003PA000900.

Sagoo, N., P. Valdes, R. Flecker, and L. J. Gregoire (2013), The Early Eocene equable climate problem: Can perturbations of climate model parameters identify possible solutions?, *Philos. Trans. R. Soc., A*, *371*(2001), doi:10.1098/rsta.2013.0123.

Scher, H. D., and E. E. Martin (2006), Timing and climatic consequences of the opening of Drake Passage, *Science*, *312*(5772), 428–430.

Schouten, S., M. J. E. C. Van Der Maarel, R. Huber, and J. S. S. Damste (1997), 2,6,10,15,19-Pentamethylicosenes in *Methanolobus bombayensis*, a marine methanogenic archaeon, and in *Methanosarcina mazei*, *Org. Geochem.*, *26*(5–6), 409–414.

Schouten, S., M. J. Hoefs, M. P. Koopmans, H.-J. Bosch, and J. S. Sinninghe Damsté (1998), Structural characterization, occurrence and fate of archaeal ether-bound acyclic and cyclic biphytanes and corresponding diols in sediments, *Org. Geochem.*, *29*(5), 1305–1319.

Schouten, S., E. C. Hopmans, E. Schefuß, and J. S. Sinninghe Damsté (2002), Distributional variations in marine crenarchaeotal membrane lipids: A new tool for reconstructing ancient sea water temperatures?, *Earth Planet. Sci. Lett.*, *204*(1), 265–274.

Schouten, S., S. G. Wakeham, E. C. Hopmans, and J. S. S. Damsté (2003), Biogeochemical evidence that thermophilic archaea mediate the anaerobic oxidation of methane, *Appl. Environ. Microbiol.*, *69*(3), 1680–1686.

Schouten, S., E. C. Hopmans, and J. S. Sinninghe Damsté (2013), The organic geochemistry of glycerol dialkyl glycerol tetraether lipids: A review, *Org. Geochem.*, *54*, 19–61.

Self-Trail, J. M., D. S. Powars, D. K. Watkins, and G. A. Wandless (2012), Calcareous nannofossil assemblage changes across the Paleocene–Eocene Thermal Maximum: Evidence from a shelf setting, *Mar. Micropaleontol.*, *92*, 61–80.

Shah, S. R., G. Mollenhauer, N. Ohkouchi, T. I. Eglinton, and A. Pearson (2008), Origins of archaeal tetraether lipids in sediments: Insights from radiocarbon analysis, *Geochim. Cosmochim. Acta*, *72*(18), 4577–4594.

Sijp, W. P., M. H. England, and J. Toggweiler (2009), Effect of ocean gateway changes under greenhouse warmth, *J. Clim.*, *22*(24), 6639–6652.

Sijp, W. P., M. H. England, and M. Huber (2011), Effect of the deepening of the Tasman Gateway on the global ocean, *Paleoceanography*, *26*, PA4207, doi:10.1029/2011PA002143.

Sijp, W. P., A. S. von der Heydt, H. A. Dijkstra, S. Flögel, P. M. J. Douglas, and P. K. Bijl (2014), The role of ocean gateways on cooling climate on long time scales, *Global Planet. Change*, *119*, 1–22.

Sinninghe Damsté, J. S., J. Ossebaar, S. Schouten, and D. Verschuren (2012), Distribution of tetraether lipids in the 25-ka sedimentary record of Lake Challa: Extracting reliable TEX$_{86}$ and MBT/CBT palaeotemperatures from an equatorial African lake, *Quat. Sci. Rev.*, *50*, 43–54.

Sivan, O., D. P. Schrag, and R. W. Murray (2007), Rates of methanogenesis and methanotrophy in deep-sea sediments, *Geobiology*, *5*(2), 141–151.

Sluijs, A., and H. Brinkhuis (2009), A dynamic climate and ecosystem state during the Paleocene-Eocene Thermal Maximum-inferences from dinoflagellate cyst assemblages at the New Jersey Shelf, *Biogeosci. Discuss.*, *6*(3), 1755–1781.

Sluijs, A., S. Schouten, M. Pagani, M. Woltering, H. Brinkhuis, J. S. S. Damsté, G. R. Dickens, M. Huber, G.-J. Reichart, and R. Stein (2006), Subtropical Arctic Ocean temperatures during the Palaeocene/Eocene thermal maximum, *Nature*, *441*(7093), 610–613.

Sluijs, A., H. Brinkhuis, S. Schouten, S. M. Bohaty, C. M. John, J. C. Zachos, G.-J. Reichart, J. S. S. Damsté, E. M. Crouch, and G. R. Dickens (2007), Environmental precursors to rapid light carbon injection at the Palaeocene/Eocene boundary, *Nature*, *450*(7173), 1218–1221.

Sluijs, A., S. Schouten, T. H. Donders, P. L. Schoon, U. Röhl, G.-J. Reichart, F. Sangiorgi, J.-H. Kim, J. S. S. Damsté, and H. Brinkhuis (2009), Warm and wet conditions in the Arctic region during Eocene Thermal Maximum 2, *Nat. Geosci.*, *2*(11), 777–780.

Sluijs, A., P. Bijl, S. Schouten, U. Röhl, G.-J. Reichart, and H. Brinkhuis (2011), Southern ocean warming, sea level and hydrological change during the Paleocene-Eocene thermal maximum, *Clim. Past*, *7*(1), 47–61.

Sluijs, A., L. van Roij, G. J. Harrington, S. Schouten, J. A. Sessa, L. J. LeVay, G. J. Reichart, and C. P. Slomp (2013), Extreme warming, photic zone euxinia and sea level rise during the Paleocene/Eocene Thermal Maximum on the Gulf of Mexico Coastal Plain; connecting marginal marine biotic signals, nutrient cycling and ocean deoxygenation, *Clim. Past Discuss.*, *9*(6), 6459–6494.

Sriver, R. L., and M. Huber (2007), Observational evidence for an ocean heat pump induced by tropical cyclones, *Nature*, *447*(7144), 577–580.

Stadnitskaia, A., D. Nadezhkin, B. Abbas, V. Blinova, M. Ivanov, and J. Sinninghe Damsté (2008), Carbonate formation by anaerobic oxidation of methane: Evidence from lipid biomarker and fossil 16S rDNA, *Geochim. Cosmochim. Acta*, *72*(7), 1824–1836.

Stickley, C. E., H. Brinkhuis, S. A. Schellenberg, A. Sluijs, U. Röhl, M. Fuller, M. Grauert, M. Huber, J. Warnaar, and G. L. Williams (2004), Timing and nature of the deepening of the Tasmanian Gateway, *Paleoceanography*, *19*, PA4027, doi:10.1029/2004PA001022.

Taylor, K. W., M. Huber, C. J. Hollis, M. T. Hernandez-Sanchez, and R. D. Pancost (2013), Re-evaluating modern and Palaeogene GDGT distributions: Implications for SST reconstructions, *Global Planet. Change*, *108*, 158–174.

Thiel, V., J. Peckmann, O. Schmale, J. Reitner, and W. Michaelis (2001), A new straight-chain hydrocarbon biomarker associated with anaerobic methane cycling, *Org. Geochem.*, *32*(8), 1019–1023.

Thomas, D. J., R. Korty, M. Huber, J. A. Schubert, and B. Haines (2014), Nd isotopic structure of the Pacific Ocean 70–30 Ma and numerical evidence for vigorous ocean circulation and ocean heat transport in a greenhouse world, *Paleoceanography*, *29*, 454–469, doi:10.1002/2013PA002535.

Tierney, J. E., and M. P. Tingley (2014), A Bayesian, spatially-varying calibration model for the TEX$_{86}$, *Geochim. Cosmochim. Acta*, *127*, 83–106.

Trommer, G., M. Siccha, M. T. van der Meer, S. Schouten, J. S. Sinninghe Damsté, H. Schulz, C. Hemleben, and M. Kucera (2009), Distribution of Crenarchaeota tetraether membrane lipids in surface sediments from the Red Sea, *Org. Geochem.*, *40*(6), 724–731.

van Hooidonk, R., and M. Huber (2009), Equivocal evidence for a thermostat and unusually low levels of coral bleaching in the Western Pacific Warm Pool, *Geophys. Res. Lett.*, *36*, L06705, doi:10.1029/2008GL036288.

Villanueva, L., S. Schouten, and J. S. Sinninghe Damsté (2014), Depth-related distribution of a key gene of the tetraether lipid biosynthetic pathway in marine Thaumarchaeota, *Environ. Microbiol.*, doi:10.1111/1462-2920.12508.

Wakeham, S. G., C. M. Lewis, E. C. Hopmans, S. Schouten, and J. S. Sinninghe Damsté (2003), Archaea mediate anaerobic oxidation of methane in deep euxinic waters of the Black Sea, *Geochim. Cosmochim. Acta*, *67*(7), 1359–1374.

Wakeham, S. G., E. C. Hopmans, S. Schouten, and J. S. Sinninghe Damsté (2004), Archaeal lipids and anaerobic oxidation of methane in euxinic water columns: A comparative study of the Black Sea and Cariaco Basin, *Chem. Geol.*, *205*(3), 427–442.

Weijers, J. W., S. Schouten, E. C. Hopmans, J. A. Geenevasen, O. R. David, J. M. Coleman, R. D. Pancost, and J. S. Sinninghe Damsté (2006a), Membrane lipids of mesophilic anaerobic bacteria thriving in peats have typical archaeal traits, *Environ. Microbiol.*, *8*(4), 648–657.

Weijers, J. W., S. Schouten, O. C. Spaargaren, and J. S. Sinninghe Damsté (2006b), Occurrence and distribution of tetraether membrane lipids in soils: Implications for the use of the TEX$_{86}$ proxy and the BIT index, *Org. Geochem.*, *37*(12), 1680–1693.

Weijers, J. W., K. L. Lim, A. Aquilina, J. S. Sinninghe Damsté, and R. D. Pancost (2011), Biogeochemical controls on glycerol dialkyl glycerol tetraether lipid distributions in sediments characterized by diffusive methane flux, *Geochem., Geophys., Geosyst.*, *12*, Q10010, doi:10.1029/2011GC003724.

Williams, I. N., R. T. Pierrehumbert, and M. Huber (2009), Global warming, convective threshold and false thermostats, *Geophys. Res. Lett.*, *36*, L21805, doi:10.1029/2009GL039849.

Wuchter, C., S. Schouten, M. J. L. Coolen, and J. S. Sinninghe Damsté (2004), Temperature-dependent variation in the distribution of tetraether membrane lipids of marine Crenarchaeota: Implications for TEX$_{86}$ paleothermometry, *Paleoceanography*, *19*, PA4028, doi:10.1029/2004PA001041.

Zachos, J. C., J. R. Breza, and S. W. Wise (1992), Early Oligocene ice-sheet expansion on Antarctica: Stable isotope and sedimentological evidence from Kerguelen Plateau, southern Indian Ocean, *Geology*, *20*(6), 569–573.

Zachos, J. C., S. Schouten, S. Bohaty, T. Quattlebaum, A. Sluijs, H. Brinkhuis, S. Gibbs, and T. Bralower (2006), Extreme warming of mid-latitude coastal ocean during the Paleocene-Eocene Thermal Maximum: Inferences from TEX86 and isotope data, *Geology*, *34*(9), 737–740.

Zhang, Y. G., C. L. Zhang, X.-L. Liu, L. Li, K.-U. Hinrichs, and J. E. Noakes (2011), Methane Index: A tetraether archaeal lipid biomarker indicator for detecting the instability of marine gas hydrates, *Earth Planet. Sci. Lett.*, *307*(3), 525–534.

Zhang, Y. G., M. Pagani, Z. Liu, S. M. Bohaty, and R. DeConto (2013), A 40-million-year history of atmospheric CO$_2$, *Philos. Trans. R. Soc., A*, *371*(2001), doi:10.1098/rsta.2013.0096.

Zhang, Z., Q. Yan, and H. Wang (2010), Has the Drake Passage played an essential role in the Cenozoic Cooling, *Atmos. Ocean Sci. Lett.*, *3*(5), 288–292.

Zhang, Z., K. Nisancioglu, F. Flatøy, M. Bentsen, I. Bethke, and H. Wang (2011), Tropical seaways played a more important role than high latitude seaways in Cenozoic cooling, *Clim. Past*, *7*(3), 801–813.